THE THEORETICAL ANALYSIS OF THE INTERACTION BETWEEN METHANE DEHYDROGENATION AND CARBON DIOXIDE DISSOCIATION PRODUCTS WITH Ni AND PtNi SURFACES

by

Merve Ayvaz

B.S., Chemical Engineering, Boğaziçi University, 2010

Submitted to the Institute for Graduate Studies in
Science and Engineering in partial fulfillment of
the requirements for the degree of
Master of Science

Graduate Program in Chemical Engineering

Boğaziçi University

2013

***to my dear parents*,**

ACKNOWLEDGEMENTS

I would like to express my best regards and truthful thanks to my thesis supervisor Prof. Dr. Ahmet Erhan Aksoylu for his great guidance and support to me during my study. He was always motivating me and sharing experienced knowledge with me. I am really proud to be worked with him on catalysis science and reaction engineering.

I must express my thanks to Ali Uzun for his endless support and valuable time while he was advising and helping me about Material Studio as an experienced colleague.

The graduate scholarship provided by TÜBİTAK (Bideb 2210 – Yurtiçi Yüksek Lisans Burs Programı) for my Master of Science studies deserves thankful recognition. Also, the financial support provided by TÜBİTAK through project 111M144 and by Boğaziçi University through project BOB-M6755 is greatly acknowledged.

Finally, I would like to thank to my dear mother and father for their love, care and their unique presence and strong believe on me in my whole life. This is a great honour to being dedicated this study to my parents.

ABSTRACT

THE THEORETICAL ANALYSIS OF THE INTERACTION BETWEEN METHANE DEHYDROGENATION AND CARBON DIOXIDE DISSOCIATION PRODUCTS WITH Ni AND PtNi SURFACES

Catalytic Dry Reforming of Methane (CDRM), in general sense, involves simultaneous carbon dioxide disproportionation yielding carbon monoxide and surface oxygen, methane dehydrogenation yielding hydrogen, CH_x groups and surface carbon, and, finally, reaction between surface oxygen and surface carbon that cleans the surface yielding carbon monoxide. The aim of this study is to investigate the adsorption properties of carbon dioxide and the products formed upon its dissociation, carbon monoxide and oxygen, on Ni(111) and PtNi(111) surfaces, and forming a vibrational frequency data base for methane dehydrogenation and carbon dioxide disproportination products adsorbed on Ni(111) and PtNi(111) surfaces via utilizing *ab initio* Dmol3 tool box of Accelrys Material Studio. Carbon dioxide adsorption properties was studied by placing carbon dioxide molecules on each possible adsorption sites of Ni(111) and PtNi(111) surface alloy. On both surfaces carbon dioxide adsorption energy values obtained were very close to zero due to the high amount of energy consumed during configurational change. Results of this study shows that adsorption of carbon dioxide is stronger on PtNi(111) surface alloy compared to the adsorption on Ni(111) surface. The most preferred adsorption site of carbon dioxide is bridge site both for Ni(111) surface and PtNi(111) surface alloy. Adsorptions of carbon monoxide molecule and oxygen atom were also studied on Ni(111) metal. Very strong adsorption of carbon monoxide and oxygen on Ni surface was verified. Calculated frequency data base, which is consistent with the experimental data in the literature, was tabulated and will be furtherly used in determination of the catalytically active adsorption sites on Ni and PtNi catalysts during CDRM reaction through comparative analysis of experimental FTIR-DRIFT studies performed on Ni/Al_2O_3 and Pt-Ni/Al_2O_3 catalysis.

ÖZET

METAN DEHİDROJENASYONU VE CARBON DİOKSİT AYRIŞMASI ÜRÜNLERİ İLE Ni ve PtNi YÜZEYLERİ ARASINDAKİ ETKİLEŞİMİN TEORİK ANALİZİ

Methanın katalitik kuru reform reaksiyonu, genel anlayış içerisinde eş zamanlı olarak, karbon dioksit ayrışmasıyla carbon monoksit ve yüzey oksijeni oluşumunu, methan dehidrojenasyonuyla hidrojen, CH_x grupları ve yüzey karbonu oluşumunu, ve, son olarak, yüzeyi karbon monoksit oluşturarak temizleyen yüzey oksijeni ile yüzey karbonu arasındaki reaksiyonu içerir. Bu çalışmanın amacı, Accelrys Material Studio'nun *ab initio* Dmol3 araç kutusu kullanılarak, karbon dioksitin ve onun parçalanması ile oluşan ürünlerin, karbon monoksit ve oksijen, Ni(111) ve PtNi(111) yüzeylerindeki adsorpsiyon özelliklerini incelemek, ve Ni(111) ve PtNi(111) yüzeylerinde adsorbe olan methan dehidrojenasyonu ve karbon dioksit ayrışması ürünleri için bir vibrasyonel frekans veri tabanı oluşturulmasıdır. Karbon dioksitin adsorpsiyon özellikleri Ni(111) ve PtNi(111) yüzey alışımı üzerindeki tüm olabilecek adsorpsiyon sitelerine karbon dioksit molekülü yerleştirilerek çalışılmıştır. Her iki yüzey üzerinde karbon dioksit adsorpsiyon enerjisi değerleri, konfigürasyonel değişim sırasında harcanan enerjiye bağlı olarak sıfıra çok yakın olarak elde edilmiştir. Çalışma sonuçları karbon dioksit PtNi(111) yüzey alaşımına Ni(111) yüzeyine tutunduğundan daha güçlü tutunduğunu göstermektedir. Karbon dioksitin en çok tercih ettiği adsorpsiyon sitesi hem Ni(111) yüzeyi hem de PtNi(111) yüzey alaşımı için "bridge" sitesidir. Karbon monoksit ve oksijen adsorpsiyonu Ni(111) metali üzerinde çalışılmıştır. Karbon monoksit ve oksijenin Ni yüzeyi üzerindeki çok güçlü adsorbe olduğu doğrulanmıştır. Literatürdeki deneysel veriler ile uyumlu olan, hesaplanmış frekans veri tabanı tablolanmıştır ve ileride CDRM reaksiyonu sırasında Ni ve PtNi katalizörlerinin katalitik olarak aktif adsorpsiyon sitelerinin belirlenmesinde, Ni/Al_2O_3 ve $Pt\text{-}Ni/Al_2O_3$ katalizörleri üzerinde yapılmış deneysel FTIR-DRIFT çalışmalarından elde edilmiş frekans değerlerinin karşılaştırmalı analizi yoluyla kullanılacaktır.

TABLE OF CONTENTS

LIST OF FIGURES

LIST OF TABLES

LIST OF SYMBOLS

Å	Armstrong
C(t)	Time dependent factor
E	Total Energy
E_{coul}	Coulomb repulsion between electrons
E_{ext}	External potential
E_{xc}	Exchange-correlation functional
M	Mass
P	Momentum
T_s	Kinetic energy functional
U(r)	Potential
V_{ext}	External Potential
χ_i	Electron orbital
Ψ	Wave function
Φ	Hartree Fock wave function
$\widehat{H}$	Hamiltonian operator
$\vec{r}$	Vector point in space
$\rho(\vec{r})$	Electron density
F	Kinetic and interaction energy
$E_{xc}(\rho)$	Exchange-correlation energy per particle

LIST OF ACRONYMS/ABBREVIATIONS

AE	All electron
AER	All electron relativistic
CDRM	Catalytic dry reforming of methane
DFT	Density functional theory
DRM	Dry reforming of methane
FCC	Face centered cubic
FTIR	Fourier transform infrared spectroscopy
GGA	Generalized-gradient approximation
HCP	Hexagonal closed packed
HF	Hartree-Fock Theory
HOMO	Highest occupied molecular orbital
IR	Infrared
LDA	Local density approximation
LDOS	Local density of state
LUMO	Lowest unoccupied molecular orbital
ME	Micro emulsion method
MLE	Mono layer equivalent
MM	Molecular mechanics
MS	Material Studio
PAW	Projector augmented-wave functional
PBE	Perdew-Burke-Ernzerhof Functional
PWC	Perdew-Wang Functional
QM	Quantum mechanics
SCF	Self-consistent field
STM	Scanning electron microscopy
TEM	Transmission electron microscopy
TPO	Temperature programmed oxidation
VASP	The Vienna Ab-initio Simulation Package
WGS	Water gas shift
XRD	X-ray diffraction

1. INTRODUCTION

Environmental concerns and depletion of fossil fuel resources motivate researchers in various fields to develop an efficient, clean and cheap alternative energy sources and ways of energy production (Padama *et al.,* 2012). During recent years the catalytic carbon dioxide reforming of methane (CDRM) process, which converts two of the cheapest and the most potent carbon-containing "greenhouse" gases (CH_4 and CO_2) into a useful chemical product (syngas), has received considerable attention. Syngas can be preferentially used for the synthesis of liquid hydrocarbons in the Fischer–Tropsch synthesis network and the synthesis of a variety of chemicals including methanol, ammonia, olefin, etc. Although CDRM reaction is endothermic, it produces synthesis gas with low H_2/CO ratio (1/1). This method offers certain advantages over other technologies, e.g. steam reforming or partial oxidation. One of these advantages is the fact that not only CH_4 but also CO_2, both of which are greenhouse gases, are consumed in the reaction. Secondly, a lower H_2/CO ratio is obtained, which is preferable for the synthesis of long chain hydrocarbons having olefinic bonds and oxygenated derivatives. Thirdly, CDRM can be used as an efficient way of chemical energy transmission (Akpan *et al.,* 2007, Fidalgo *et al.*, 2010, Quiroga and Luna, 2010, Wang *et al.,* 2006, Zhu *et al.,* 2009).

Due to the high efficiency of hydrogen oxidation in fuel cells and its cleanness, hydrogen is considered to be one of the most promising alternative fuels. Hydrogen may be produced by several ways including reforming of hydrocarbons and alcohols, gasification of coal or biomass and the electrolysis or thermochemical decomposition of water (Wang *et al.,* 2010). Between methane reforming methods, steam reforming of methane (SRM) is used industrially for large-scale hydrogen production. However, hydrogen production at a smaller scale from fossil fuels requires further investigation. In this regard, CDRM, when it is followed with WGS in a membrane reactor, could be the key if the process is to meet the requirements of purity, economics and versatility to be integrated fuel processor and fuel cells systems. CDRM inconjunction with the water-gas-shift (WGS) reaction may be applied to produce hydrogen. Up to now, only a small fraction of the hydrogen produced is

currently used for energy process, but the implementation of fuel cell systems and the growing demand for zero-emission fuels in the near future will increase the hydrogen share in the energy market Its production from abundant sources such as natural gas in an economical way and with reduced purification cost would help to make the commercialization of fuel-cell-powered systems possible (Akpan *et al.,* 2007).

The adsorption and reaction of hydrogen and hydrocarbon fragments on catalytically active transition metal surfaces have been extensively studied due to the commercial importance of hydrocarbon formation reactions. Methane is the least reactive alkane, so the adsorption of methane on transition metal surface has been also studied extensively by theoreticians. Surface reactions of methane on nickel surfaces have been studied extensively, since these reactions are involved in industrially important reactions, such as steam reforming of methane and methanation of carbon monoxide (Zuo *et al.*, 2010, Michaelides and Hu, 2000b, Watwe *et al.,* 2010).

From the industrial standpoint, nickel is the most appropriate catalyst for the methane reforming reaction, due to its availability and low cost. However, the Ni-based catalysts are promptly deactivated by the deposition of carbon on their active centers. In general, there are two approaches for minimizing coke formation. The first one is to optimize process conditions such as to suppress coke formation; i.e. the use of high temperatures, low space velocities and diluted feed. The second approach is the modification of the in catalysts (Ito *et al,* 1999, Pietraszek *et al.,* 2011, Pistonesi *et al.,* 2007, Quiroga and Luna, 2010).

The major issue encountered in the application of CDRM process is the rapid deactivation of the nickel-based catalyst, mainly by carbon deposition. The development of robust nickel-based catalysts, which are resistant to carbon deposition and which will exhibit stable operation for an extended period of time is urgently needed (Akpan *et al.,* 2007). To minimize the deposition of carbon on the catalyst, it has been suggested that the catalyst should be designed to avoid large ensembles of the metal species that facilitates carbon formation. In general, precious metals such as Rh, Ru, Pd, Pt, and Ir can lead to lower carbon deposition in the CH_4 reaction (Zuo *et al.*, 2010). Pt is one of the mostly

studied noble metal to reduce carbon deposition on Ni catalyst for methane reforming reactions. On Pt-modified Ni catalyst, Pt is either incorporated to the Ni surface forming Pt-Ni surface alloys and/or Pt forms small clusters in the closed vicinity of Ni islands. Pt atoms can contribute to the enhanced reducibility and keep Ni species in metallic form under the presence of oxygen. However, some kind of synergy occurs between Ni and Pt on the alumina carrier, yielding improved dry methane reforming activity (Dieguez et al., 2010a, Li *et al.,* 2007, Pawelec *et al.,* 2007).

The aim of this thesis is to investigate the adsorption properties of CO_2 and the products formed upon its dissociation, CO and O, on Ni(111) and PtNi(111) surfaces, and forming a vibrational frequency data base for methane dehydrogenation and CO_2 disproportionation products adsorbed on Ni(111) an PtNi(111) surfaces via utilizing *ab initio* DMol3 tool box of Accelrys Material Studio. In chapter two, experimental and theoretical studies of CDRM in literature are summarized. The information on the types of CDRM catalyst studies experimentally and theoretically are presented in this section. Additionally, frequency values of the reactants, reaction intermediates and products of CDRM reaction on Ni and PtNi surfaces are also gathered from the literature and presented in chapter two. In chapter three, theoretical background behind the density functional theory and DMol3 tool box of Material Studio are explained. The adsorption values of CO_2 and the products formed upon its dissociation, CO and O, are given in chapter four together with the calculated frequency data for CH_x species, CO_2, CO and O. LDOS profiles and preferred adsorption sites on Ni(111) metal and PtNi(111) surface alloy can be also found in fourth chapter. Conclusion and recommendations for further studies are made in Chapter 5.

2. LITERATURE SURVEY

During recent years catalytic dry reforming of methane (CDRM) producing synthesis gas (hydrogen and carbon monoxide) has received a lot of attention, as it offers certain advantages over other alternative technologies, e.g. steam reforming or partial oxidation. The dry reforming reaction (Equation 2.1) is accompanied by several side reactions, which the reverse water–gas shift (Equation 2.2), methane cracking (Equation 2.3) and the Boudouard reaction (Equation 2.4) appears to be the most important ones.

CDRM permits to obtain a syngas mixture with H_2/CO product ratio near to one. Generation of synthesis gas with a low H_2/CO ratio can be preferentially used for the production of liquid hydrocarbons in the Fischer Tropsch synthesis network. Calculations indicate that dry reforming reaction is thermodynamically favored above 640 ^{o}C. It is more endothermic than steam reforming and partial oxidation. Numerous metals like Ni, Co, Fe or Nobel metals (Pt, Rh, Pd, Ir) have been reported to be active for CDRM (Fidalgo *et al.*, 2010, Luna and Iriarte, 2008, Parvary *et al.*, 2001, Dieguez *et al.,* 2010a).

$$CH_4 + CO_2 \rightarrow 2CO + 2H_2 \quad (2.1)$$

$$CO_2 + H_2 \rightarrow CO + H_2O \quad (2.2)$$

$$CH_4 + C \rightarrow 2H_2 \quad (2.3)$$

$$2CO + C \rightarrow CO_2 \quad (2.4)$$

Alumina-supported Ni catalysts are the most widely used catalysts for catalytic reforming of methane with carbon dioxide or steam for hydrogen production due to their low cost and high activity. Considering the low cost and availability of nickel, it is more practical to improve the properties of Ni-catalysts such as to exhibit fast turn over and stable operation from an industrial point of view. The nickel catalysts are deactivated quickly due to the formation of coke on the surface of the active phase, poisoning and structural transformation, sintering and recombination of the active components under

endothermic reaction conditions. In this case, Ni catalysts doped with small amounts of noble metals are reported to display an ‘‘intelligent” behavior, with suppression of such deactivation phenomena. Another method is using bimetallic structure (Ni-Mn; Ni-Fe) or addition of alkali earth or rare earth to reduce carbon formation. Formation of bimetalic structure with Al or Mg has been attracted attention (Dieguez *et al.*, 2010a , Parvary *et al*., 2001, Pawelec *et al*., 2007).

2.1. Proposed Mechanism of CDRM on Ni Catalysts

The reaction mechanism of dry reforming of methane on Ni(111) was investigated by calculations based on density functional theory (DFT) with PAW method in VASP code in the study of *Zhu et al., 2009*. The used functional is GGA-PBE. The free energy barriers for the direct CO_2 decomposition and H-induced CO_2 decomposition are calculated to be 2.13 eV and 2.40 eV, respectively. Therefore, CO_2 is predicted to dissociate via a direct pathway to generate CO and O dominantly, and atomic O is taken as the primary oxidant of CH_x intermediates. However, the H-induced CO_2 decomposition contributes to dry methane reforming as well because of the comparable barriers, and the effect of the oxidant OH is not negligible. As for these two dominant reaction pathways, the oxidation step is predicted to determine the overall reaction rate at 973.15 K while the CH_4 dehydrogenation is found to be the rate limiting step at lower temperatures. The reaction network begins with the CO_2 decomposition to generate O as could be seen in Figure 2.1 and agreed with the study of *Wang et al., 2007*.

Density functional theory calculation with Material Studio Package is used to investigate reaction pathways of dry reforming of methane on Ni(111) in the study of *Wang et al., 2007*. GGA and PBE functional are used in CASTEP tool of Material Studio. A new and simplified mechanism was proposed on the basis of computed energy barriers, confirmation of the computed kinetic parameters with the available experimental data.

The first step of the investigated new mechanism is CO_2 dissociation into surface CO and O ($CO_2 \rightarrow CO + O$) and sequential dissociation of CH_4 into surface CH and hydrogen ($CH_4 \rightarrow CH_3 \rightarrow CH_2 \rightarrow CH$). CH oxygenation is the second step; CH gets O and

turn into CHO (CH + O → CHO), which is more favored than its dissociation into surface C and hydrogen (CH →C + H). The third step is the dissociation of CHO into surface CO and H (CHO → CO + H). Finally, H_2 and CO desorb from Ni(111) and form free H_2 and CO (Wang *et al.*, 2007, Zhu *et al.*, 2009).

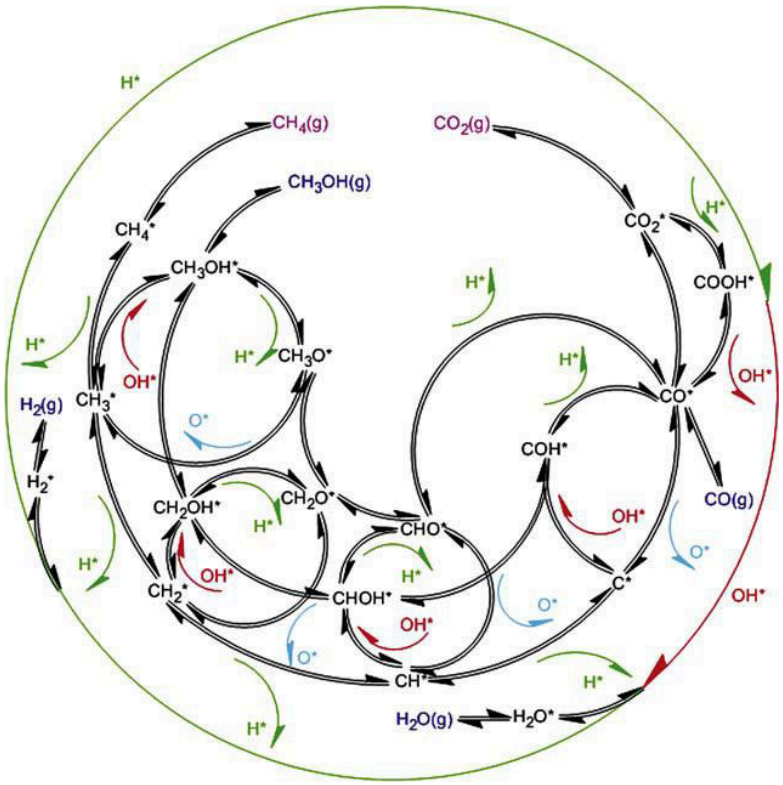

Figure 2.1. Proposed reaction mechanism of dry reforming of methane on Ni catalyst.

The dissociation of methane on the terraces and steps of a Ni(111) surface was theoretically and experimentally investigated. The DACAPO code was used for all total energy calculations. The intrinsic sticking probability for terraces is smaller than for steps at 500 K regarding to experimental results. Corresponding to an activation energy difference of 20 kJ/mol, which is identical to the results obtained from the DFT calculations (Pedersen *et al.*, 2005).

2.2. Several Ni Containing Catalysts and Their Performance for Methane Reforming

Metal catalysts promoted with Ce were investigated for their catalytic activity. In the study of *Pietraszek et al., 2011* , mixed sol–gel and impregnation method were used to synthesize 5 wt %Ni/CeZr 0.5 wt %Me (Rh, Ru) catalysts. XRD, TPO, TEM and Raman were used in characterizing the aged catalysts. It was found that Ni/CeZrRh catalyst demonstrated the highest activity at 800 ^{o}C with a CH_4 conversion near the thermodynamic boundary. The stability of Ni/CeZr catalyst increases with the presence of noble metals. In the study of *Aydinoglu et al., 2009,* Pt-Ce/ZrO_2 catalyst having 1 wt % Ce led to the highest catalytic activity and stability among the catalysts with different Ce loadings. The reason for high activity was explained by the intensive interaction between Pt and Ce phases for coimpregnated sample, which had been verified by X-ray photoelectron spectroscopy and Energy Dispersive X-Ray analyses. On the other hand, under severe reaction conditions, like CH_4:CO_2=2:1 reactant ratio case, it is observed that 1 wt.% Pt–5 wt.% Ce/ZrO_2 catalyst prepared by coimpregnation method displayed the most favorable stability profile (Aydinoglu *et al.*, 2009, Pietraszek *et al.*, 2011).

A series of Pt-Ni bimetallic catalysts supported on δ-Al_2O_3 was tested to optimize the Ni/Pt metal composition. The activity results show that the catalytic performance of bimetallic Pt-Ni samples strongly depended on the metal loadings and Ni/Pt loading ratio. Among all the catalysts, 0.3% Pt - 10% Ni/Al_2O_3, which has the lowest Ni/Pt ratio, exhibited the highest catalytic activity and stability (Aydinoglu and Aksoylu, 2011).

Mineral clay (Si_2O_5) modified with Al was used as support of praseodymium promoted bimetallic Pr-Ni catalyst to use in dry reforming of methane. Diverse works have demonstrated that coke formation can be reduced when there is a greater dispersion of metal and when basic precursors and/or redox type promoters are employed. Among the redox type promoters, the use of Pr has recently been reported because of its great capacity of O_2 storage. It is assumed that the role of Pr is based on the generation and promotion of superficial oxygen features and oxygen vacancies, which in the environs of metallic particles promote the removal of carbon from the metallic surface by means of a mechanism in which the redox pair Pr^{3+}/Pr^{4+} participates. The catalysts with 3% Pr register

the highest conversions which are found to be between 44% and 55% for the CH_4 and CO_2, respectively. The catalyst with 5% Pr registered conversions that were equal to or, in some cases, lower than those obtained for the catalysts with 3% Pr. This behavior suggests the existence of a maximum in the ratio quantity of Pr/dispersion, indicating that with 3% Pr the greatest quantity of Pr available with the smallest particle size; while at greater quantities (5%) the size of the particle aggregates surely gets larger (Gamba *et al.*, 2011).

Recently, supported nickel catalysts Ni/Al_2O_3 and $Ni/MgO–Al_2O_3$ with core/shell structures were tested for CDRM. Supported Ni catalysts with 10% Ni loading on Al_2O_3 and $MgO–Al_2O_3$, which have the best performance in the steam reforming of methane (97% methane conversion at 750 °C) and in the partial oxidation of methane (96% methane conversion at 800 °C), show also excellent thermal stability for CDRM in the first 150 h. Additionally, $Ni/MgO–Al_2O_3$ catalyst has lower carbon deposition compare to that on Ni/Al_2O_3 catalyst (Kang *et al.*, 2011).

Several Co–Mo and Ni–Mo carbide catalysts have been studied in order to find out the effect of cobalt or nickel content of molybdenum carbide CDRM catalysts on the dry reforming performance. The results indicate that incorporating cobalt into the Mo_2C structure at a Co/Mo ratio of 0.4 gives activity and stability that are markedly higher than those of Mo_2C catalysts. A Ni/Mo atom ratio of 0.2 gives the maximum synergistic interaction between Ni and Mo for the Ni-Mo carbide catalyst (Cheng *et al.*, 2010).

Alumina supported Ni, Co and bimetallic Co-Ni catalysts (with 9 wt. % nominal metal content) have been characterized and tested for their performance in CDRM. The bimetallic catalysts show higher activity and stability due to synergistic effect between the two metals as producing non-deactivating carbon deposits. The remarkable stability of the Co rich catalysts seems to be related with the presence of large particles, which are involved in long-term conversion because they produce non-deactivating carbon deposits. It is noted that although Co rich catalysts show good catalytic properties, they should be improved to hinder carbon deposition (Alonso *et al.*, 2009).

2.3. Frequency Data Obtained on Ni Metal Surface and PtNi Surface Alloy

Nanostructured PtNi catalysts, prepared by the reverse microemulsion method (ME) and supported on a nanofibrous alumina, were tested for the CO_2-reforming of methane. Through using the ME method and the nanofibrous support, it is possible to obtain systems with homogeneous and well dispersed particles of Ni and/or Pt. The addition of Pt in Ni-based catalysts and the preparation of the catalysts by ME inhibits global carbon formation, promotes the relative content of active species, suppresses metal sintering, and improves the stability of the catalysts considerably (Dieguez *et al.*, 2010b).

The catalytic data reported for bimetallic PtNi catalysts supported on a nanostructured c-Al_2O_3 together with the corresponding monometallic materials, employed for the dry reforming of methane, show that the monometallic 0.4Pt/Al_2O_3 catalyst is slightly more active than the 4Ni/Al_2O_3 catalyst in spite of the smaller metal content, which is in agreement with the intrinsically higher activity of platinum with respect to nickel in the reaction. However, an improvement in the catalyst activity can be obtained not only by introducing a small amount of Pt on the Ni/Al_2O_3 catalyst (0.04Pt4Ni/Al_2O_3 catalyst) but also through adding a significant amount of Ni to the Pt/Al_2O_3 catalyst (0.4Pt4Ni/Al_2O_3 catalyst). It is evident that some kind of synergy occurs between Ni and Pt on the alumina carrier, improving DRM activity in terms of conversion (Dieguez *et al.*, 2010a).

In the study of *Dieguez et al.,2010a,* IR spectrums were investigated. In the spectra of surface species arising from CO adsorption over the reduced 4Ni/Al_2O_3 catalyst, two well-resolved bands were detected at 2017 and 1907 cm^{-1} at room temperature, and at 2184 and 2167 cm^{-1} at low temperature. In the spectra of surface species arising from CO adsorption over the reduced 0.4Pt4Ni/Al_2O_3 catalyst, main band that shifts from 2079 to 2064 cm^{-1} by increasing temperature upon outgassing is definitely similar to that of terminal carbonyls on Pt crystal faces. However, the position of this band is clearly shifted up with respect to that observed on the 0.4Pt/Al_2O_3 catalyst (2069–2054 $cm^{-}1$). This is certainly an effect of the presence of Ni species. Additionally, easier reduction of Ni species led by the presence of Pt is proposed.

Vannice studied CO adsorption on Ni(111) at low coverages and observed that a predominant band is shifting from 1830 to 1900 cm^{-1} depending on the coverage, traditionally assigned to bridging CO. A weaker band at 1796–1825 cm^{-1} usually attributed to hollow adsorbed molecules (triply bridging) together with weak bands due to terminal carbonyls, at 2030–2060 cm^{-1}, depending on the coverage. According to *Yoshinobu and Kawai*, on Ni(100) at 20 K and very low coverage, the bands of terminal and bridging CO are observed at 2019–2029 cm^{-1} and 1863–1875 cm^{-1}, respectively and the latter split at higher coverages. At room temperatures, these features were found at 2016 and 1935 cm-^{1}. A similar situation was found for CO on Ni(311) (Vannice, 1982, Schilbe et al., 1995, Yoshinobu and Kawai, 1996, Formonso et al., 2006).

In a theoretical work, periodic infinite plane wave slab calculations were performed, in conjunction with density functional theory and ultrasoft pseudopotentials to study the adsorption of CH*x* (*x*D1, 2, 3) species on the Ni(111) surface. It is found that the three-fold hollow site is the stable site for CH adsorption on Ni(111) and the C–H stretching frequency to be 3035 cm^{-1}, which is in agreement with the experimental value of 2970 cm^{-1}. Methyl species (CH_3) are found to adsorb on threefold hollow sites with H atoms pointing toward Ni atoms. C–H stretching frequency of CH_3 was calculated to be 2730 cm^{-1}, which is in agreement with the experimental value of 2655 cm^{-1}. As a consistant of *Yang and Whitten, 1996*, the CH stretching band, which is not detected by IRAS, is observed at 2965 cm^{-1} using off-specular HREELS (Watwe et al., 2000, Yang and Whitten, 1996).

2.4. DFT Studies of Dry Reforming of Methane on Ni Catalysts

DFT is utilized to evaluate behavior of reactants and products, and the surface interactions on Ni(111) as well, through the use of several computational packages like VASP, CASTEP and ADF2004.01. CO_2 is predicted to dissociate via a direct pathway to generate CO and O dominantly, and atomic O is taken as the primary oxidant of CHx intermediates. The reaction network begins with the CO_2 decomposition to generate O and the CH_4 dehydrogenation to produce CH and C, which are subsequently oxidized by atomic O to form CHO and CO, and ends with the decomposition of CHO to produce CO

and H_2. As for these two dominant reaction pathways, the oxidation step is predicted to determine the overall reaction rate, while the CH_4 dehydrogenation is found to be the rate limiting step at lower temperatures. CO adsorbs on top of Ni atom through C atom, weakening the involved surface Ni–Ni bonds. H atom bonds to three-fold surface site and similarly weakens the neighboring Ni–Ni bonds. It was found that carbon formation on Ni(111) is disfavored kinetically. Both surface H and O can eliminate carbon deposition, but surface H has higher ability than surface O. This agrees with the fact that the more H_2 exists and the less carbon deposition forms in steam reforming than in CO_2 reforming system (Aydinoglu and Aksoylu., 2011, Pistonesi *et al.*, 2007, Wang *et al.*, 2007).

The adsorption of CH_3 and CH_2 on Ni(111) was studied *ab-initio* by utilizing density functional calculations. The total energy program, CASTEP was used throughout the study to obtain optimized structures and energies. Calculated adsorption energies of CH_3 on the different sites are in the following order: hcp>fcc>bridge>top. Adsorbed CH_3 exhibits lengthened C-H bond and the exact length of these bonds depends on the adsorption site. These lengthened C-H bonds are one of the major reasons of soft C-H vibration. They occur because there is three-centre bonding between C-H-Ni. When CH_3 is initially placed on an fcc site, one of the C–H bonds is stretched and CH_3 translates towards a bridge site accessing an identical transition state. After the transition state, the CH_2 and H fall into neighboring fcc sites. In this pathway, the C moiety, therefore, also makes an unusual movement through translating from an fcc threefold hollow site towards a bridge site and then back again to the same fcc site. According to the published data, CH_3 was suggested to favor top sites, CH_2 to bridge sites and CH to hollow sites, whereas H binds strongly at threefold hollow sites. CH_2 adsorbs strongly at the fcc, hcp, bridge and top sites, respectively. In the case for CH_3 adsorbed on Ni (111), C-H-Ni three-center bonding has been detected. In the CH_2-H coadsorption systems the adsorbates have a tendency to move toward bridge sites. The activation energy for the lowest energy reaction pathway identified is 1.06 eV (Michaelides and Hu, 1999, Michaelides and Hu, 2000a, Michaelides and Hu, 2000b).

Density functional theory calculations were also performed to investigate C adsorption and diffusion on the surfaces and in the subsurfaces of nonreconstructed and

reconstructed Ni (100). The self consistent total energy calculations based on DFT are performed with use of the VASP code. It is found that C atoms bind most strongly to the fourfold hollow sites. At low coverages, C atoms tend to accumulate on the surface to a higher level because of the relatively slow diffusion rate. When the critical coverage is attained, the surface reconstruction takes place and promotes the C diffusion dramatically (Zhu *et al.*, 2007).

3. METHODOLOGY

In electron diffraction, the wave nature of the electron is evident from its behavior upon interaction with periodic array of atoms in crystal. By contrast, in photoelectric effect, where a single photon ejects a single electron, the behavior of both the photon and the electron may be understood from a particle viewpoint. Different experiments may be interpreted by either a wave or a particle model, and we are left in a quandary as to which way to think about the particle, or whether different experiments require different models for the particle, or more interestingly, whether the particle has a dual wave and particle character (Yates and Johnson, 2007).

3.1. The Schrödinger Equation

Schrödinger's mechanics is capable of giving descriptions of energies and distributions of the electrons which determined chemical structures and processes of arbitrary accuracy (Cook, 2005).

The electron as a wave is described as total wave function, Ψ, which is a function of both time and position and is therefore traveling wave. A centrally important postulate of wave mechanics is that the quantity Ψ* Ψ is proportional (for a given particle energy) to the number of particles that cross a unit area per unit time. The wave function, Ψ, contains a time-dependant factor, C(t), which is essential for describing a travelling wave. A second factor, Ψ(x,y,z), is time-independent, and depends only on the coordinates within the system. Thus Ψ= C(t) Ψ(x,y,z).

Schrödinger studied de Broglie's paper in 1925 and then went on to develop a wave function model, which is widely employed basis for all quantum mechanics. His wave equation is now called the Schrödinger's equation, which can be completely written as Equation 3.1. $\widehat{H}$ is the so-called Hamiltonian operator, and E is the total energy of the system (Yates and Johnson, 2007).

$$\hat{H}\Psi = \mathrm{E}\Psi \tag{3.1}$$

Hamiltonian Equation forms a system of differential equations and may thus apply the ordinary theory of existence and uniqueness of solutions to them. There, simplifying assumptions will be always made that every solution exists for all times, and is unique. This is, for instance, always the case when the Hamiltonian is the type like seen in Equation 3.2.

$$H = \frac{1}{2m}p^2 + U(r) \tag{3.2}$$

Where, p is the momentum of the particle, m is the mass and the potential U satisfies a lower bound of the type $U(r) \geq A - Br^2$ where B≥0, and this condition is actually satisfied in many case (Gosson, 2001).

3.2. Quantum Mechanical Modeling

The goal of the quantum mechanical modeling is to compute the relevant physical properties of the system containing many atoms by solving the Schrödinger equation. The premise of quantum mechanical modeling is to find an approximate solution to the many body Schrödinger equation that is "close enough" to the real solution. Two distinct approaches have been developed to attack the quantum mechanical many-body problem. Simplistically, these can be categorized as either "solving an exact equation approximately" or "solving an approximate equation exactly". These two approaches are represented in the 1988 Nobel Prize in Chemistry awarded to John Pople for molecular orbital model and Walter Kohn for density functional theory (Yates and Johnson, 2007).

3.2.1. Molecular Orbital Model

The mathematical method from linear algebra is used to express the true wave function as a linear combination of an infinite series of functions, called a basis set Basis set could be truncated at some finite number of terms and solve Schrödinger equation with

this truncated wave function. Having only an approximate description of wavefunction is one of the two problems with molecular orbital approach. The second problem is more difficult to be dealt with. The basic problem is that there is no known way to solve the full Schrödinger equation for interacting electrons. Therefore, it is assumed that each electron moves in an average potential field resulting from the other electrons and the nuclei in the system, thus decoupling the many-body problem into a series of one body problems. This approximation is used in developing the Hartree-Fock equations, also called Hartree-Fock Theory (HF), which is the basis of almost all molecular orbital calculations (Yates and Johnson, 2007).

3.2.1.1. Hartree-Fock Theory. The approximation made within HF theory is that each electron moves in an average potential filed of the other electrons in the system. Hartree-Fock calculations have been used extensively in quantum mechanical calculations of molecules and solids.The Hartree Fock wavefunction, ϕ, is a single determinant of n, one-electron orbitals χ_i and the best set of X_i are to be determined by the turning points in the Hartree-Fock Functional in Equation 3.3. Since ϕ is completely fixed by the component χ_i, it is more meaningful to express E as a functional of χ_i (Cook, 2005).

$$E[\chi_i] = \frac{\int \phi * \hat{H} \phi dr}{\int \phi * \phi dr} \tag{3.3}$$

3.2.1.2. Density Functional Theory. The basis for DFT is that the properties of any atomic or molecular system can be expressed uniquely as a function of the electron density. Hohenberg and Kohn presented a rigorous proof that for any given external potential function, V_{ext}, the correct ground state energy, E, is uniquely determined by the electron density, $\boldsymbol{\rho}(\vec{\boldsymbol{r}})$, where the integration is over all volume, V_{ext}, is the external potential determined by the nuclear charges and any other external field, $\boldsymbol{\rho}(\vec{\boldsymbol{r}})$ is the electron density at any vector point in space $\vec{\boldsymbol{r}}$, and $\boldsymbol{F}[\boldsymbol{\rho}(\vec{\boldsymbol{r}})]$ is a universal functional that accounts for the kinetic and interaction energy of the electrons.

$$E[\rho(\vec{r})] = \int V_{ext}(\vec{r})\rho(\vec{r})d\vec{r} + F[\rho(\vec{r})] \tag{3.4}$$

Instead of actually solving Hohenberg and Kohn equation, so-called Kohn-Sham equations, it could be used like seen in Equation 3.4 and Equation 3.5.

$$E[\rho(\vec{r})] = T_s[\rho(\vec{r})] + E_{ext}[\rho(\vec{r})] + E_{coul}[\rho(\vec{r})] + E_{xc}[\rho(\vec{r})] \quad (3.5)$$

There, T_s is the kinetic energy functional of a noninteracting electron gas, E_{ext} is the functional for the external potential, E_{coul} is the energy due to coulomb repulsion between electrons, and E_{xc} is the exchange-correlation functional, which accounts for electron exchange and correlation effects. E_{xc} is only part that is not known exactly. As a result, DFT methods all use various approximate expressions for E_{xc} (Yates and Johnson, 2007).

3.3. Generalized Gradient Approximations to Density Functional Theory

Within density functional theory (DFT), the ground state energy of an interacting system of electrons in an external potential can be written as a functional of ground state electronic density. When compared with the conventional quantum chemistry methods, this approach is particularly appealing since it does not rely on the knowledge of the complete N- electron wave function but only of the electronic density. Several approximate exchange- correlation functional have been proposed in the literature, and the most commonly used ones being the local density approximation (LDA) and the generalized gradient approximation (GGA).

The local density approximation (Equation 3.6) is the simplest and most widely used exchange-correlation functional.

$$E_{xc}^{LDA}[\rho] = \int \rho(\vec{r})\varepsilon_{xc}^{LDA}[\rho(\vec{r})]d\vec{r} \quad (3.6)$$

Where $\varepsilon_{xc}^{LDA}(\rho)$ is the exchange-correlation energy per particle of a homogeneous electron gas of density ρ. $E_{xc}^{LDA}[\rho]$ is by definition the exact functional for a homogeneous electron gas and has been shown to give also a qualitatively good description of the ground state properties of a variety of highly inhomogeneous systems. However, LDA does not

always provide sufficiently accurate results. For example, it almost overestimates the binding energy and underestimates the bond-length of weakly bound molecules and solids.

The GGA functional (Equation 3.7) seems to give a good description of several finite systems; they significantly improve total energies of atoms, as well as binding energies and vibrational frequencies of first and second-row molecules. They also give better estimates of bond-length and binding energies of weakly bound IIA and IIB homonuclear dimmers and hydrogen bonded systems, which are greatly overbound in LDA (Seminario, 1996).

$$E_{xc}^{GGA}[\rho] = \int \rho(\vec{r})\varepsilon_{xc}^{GGA}[\rho(\vec{r}), |\nabla\rho(\vec{r})|, \nabla^2\rho(\vec{r})]d\vec{r} \quad (3.7)$$

3.3.1. DFT Calculations for Surface of Metals

DFT methods have played an important role in elucidating the mechanism of the relevant reactions on catalytic metals, zeolites and oxides and have led to improvements in the design of catalytic converters that improve their efficiency and lower their cost.

DFT has been used along with ultra-high vacuum surface science experiments such as scanning tunneling microscopy (STM), temperature programmed desorption, X-ray diffraction, and X-ray photoelectron spectroscopy to determine the surface structure of metals, metal oxides, nanoparticles, carbide, and sulfides (Sholl and Steckel, 2009).

3.3.2. Periodic Boundary Conditions and Slab Models

To study a surface, the ideal model would be a slice of material that is infinite in two dimensions and finite along the surface normal. The basic idea is illustrated in Figure 3.1 below. The supercell contains atoms along only a fraction of the vertical direction. The atoms in the lower portion of the supercell fill the entire supercell in the x and y directions, but empty space has been left above the atoms in the top portion of the supercell. This model is called a slab model since, when the supercell is repeated in all three dimensions, it

defines a series of stacked slabs of solid material separated by empty spaces (Sholl and Steckel, 2009).

3.4. Material Studio Software

Materials Studio® is a complete modeling and simulation environment that enables researchers in materials science and chemistry to develop new materials by predicting the relationships of a material's atomic and molecular structure with its properties and behavior. Using Materials Studio 6.0, researchers in many industries can engineer better performing materials of all types, including pharmaceuticals, catalysts, polymers and composites, metals and alloys, batteries and fuel cells, nanomaterials, and more (Material Studio Software, 2011).

Materials Studio 6.0 delivers a range of tools that have the modeling and simulation capabilities even for larger and more complex systems. Tools in the areas of quantum mechanics, mesoscale modeling, and polymorph prediction enable users to simulate the complexity of systems that can be modeled in the fields of nanomaterials, molecular crystals, polymers, and organic chemistry (Material Studio Release Notes, 2008).

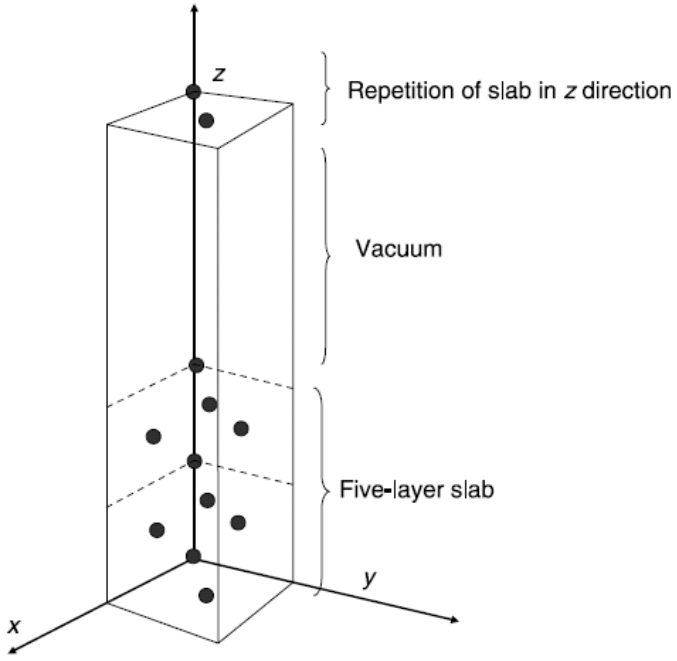

Figure 3.1. Schematic view of a periodic slab.

3.4.1. MS Visualizer and MS DMol3

Materials Studio Visualizer provides capability to construct, manipulate and view models of molecules, crystalline materials, surfaces, polymers, and mesoscale structures. It also supports the full range of Materials Studio simulations with capabilities to visualize results through images, animations, graphs, charts, tables, and textual data (Material Studio Overview, 2011).

DFT studies were performed on the structures that were designed with MS Visualizer. MS Visualizer library has ready unit cell structures for elements and also for catalysts and polymers. In this study Ni unit cell structure in the memory of MS Visualizer library is used.

Firstly geometry of bare Ni unit cell is optimized with DMol3 tool. Slab of Ni was generated on geometrically optimized Ni cell with (111) surface. The vacuum region is constructed on slab geometry after (111) face of Ni is formed. Vacuum region enable us to be sure about that there is no interaction between top of the nickel surface of interest, which adsorption and reaction kinetics are studied, and the bottom of the repeated Ni surface at z- direction of the slab. This slab structure was used to build supercell. The supercell compose of serial Ni unit cells in x and y directions. By this way, Ni surface becomes ready to be studied in adsorption and reaction kinetics studies.

Materials Studio provides a range of quantum mechanics-based tools for molecules and periodic structures, including density functional methods, linear scaling DFT, QM/MM and semi empirical tools. These tools provide accurate results for the structural, thermophysical, electronic, and optical properties of materials. DMol3 is used to model the electronic structure and properties of organic and inorganic molecules, molecular crystals, covalent solids, metallic solids, and infinite surfaces using DFT (Material Studio Overview, 2011).

In this study DMol3 tool is used to calculate adsorption energies, bond frequencies and density states of electrons. DMol3 applies DFT method in performing those calculations with quantum mechanics.

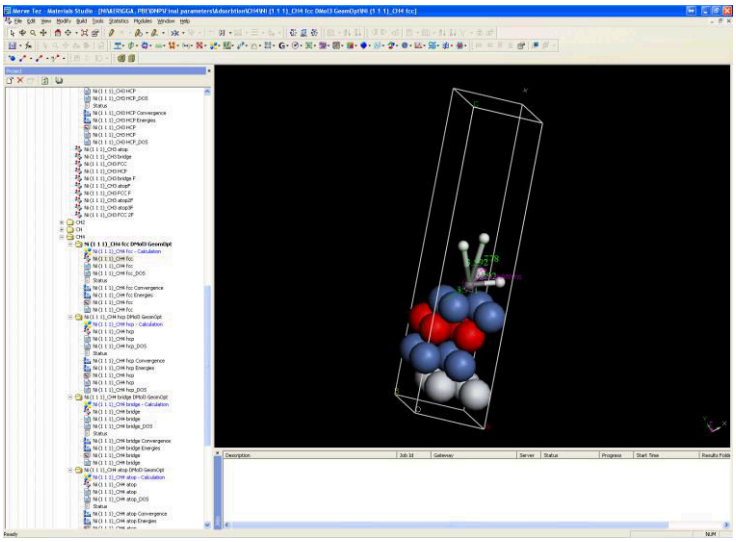

Figure 3.2. Interface of the material studio.

3.4.2. MS DMol3

DMol3 is a modeling program that uses density functional theory (DFT) to simulate chemical processes and predict properties of materials in MS. DMol3 uses localized numerical orbitals for the basis functions and each function corresponds to an atomic orbital. The basis functionals are expressed numerically as values on atomic centered spherical-polar mesh, rather than analytical Gaussian orbitals. The angular portion of each function is the appropriate spherical harmonic and the radial portion is achieved by solving the atomic DFT equations numerically. The possible optimization algorithms are not under user's control and the possible one is determined automatically depending on the system under study (Delly *et al.,* 1990; Delly *et al.,* 2000).

DMol3 is an analysis tool which is mostly used for geometry optimization task, energy task and frequency analysis. In this study, DMol3 tool is especially preferred to determine bond frequencies of the molecules, each of which has a role in the surface

reaction mechanism of CDRM, in their adsorbed state on the catalytically active centers of the CDRM catalysts, namely monometallic Ni and bimetallic PtNi.

The ready Ni structures are taken from the library of the materials studio and are cleaved in order to have (111) surface as a slab to form catalyst surface. Then, LDA is used in the frequency analysis of the adsorbed species on Ni(111) and PtNi(111), and GGA is used for analyzing the adsorption energies of the species on these surfaces.

3.5. Calculational Parameters

Spin-polarized density functional theory calculations, as implemented in the program package DMol3 in Materials Studio of Accelrys Inc. (version 6.0), were carried out in repeated slab geometry.

Since Ni(111) surface is the mostly investigated surface of Ni (Wang *et al.,* 2006) and it has been widely studied in other computational and experimental works, Ni single crystal surface was modeled by the (111) termination (Das and Shoji, 2011, Pistonesi *et al.,* 2007, Wang *et al.,* 2007; Pick *et al*., 2007; Zhu *et al.,* 2009).

In order to analyze the adsorption characteristics of the molecules which play roles in CDRM on Ni(111) surface; geometry optimization was utilized for CO_2, CO, and O adsorption on Ni(111). Also, geometry optimization was performed for CO_2 on PtNi(111) surface alloy. Adsorption energies were calculated by using Equation 4.1.

$$E_{ads} = E^{slab+adsorbate} - E^{slab} - E^{adsorbate} \quad (4.1)$$

In this study, Monkhorst-Pack special k-point sets were used for Brillouin zone integrations. 4x4x1 k-point sampling for 2x2 supercell was determined as the optimum k-point sampling after the comparative accuracy analysis. This analysis was performed for 4x4x1, 4x4x4, 6x6x6 and 8x8x8 k-point samplings. The difference in total energy of the system modeled by using 2x2 supercell was below 0.095 Ha for Ni bulk geometry optimization which was calculated by using 4x4x1 and 8x8x8 k-point samplings. The

optimum k-point sampling for 2x2 supercell was integrated to 2x3 supercell as 4x6x1 k-point sampling.

In the adsorption study of CO_2, CO, O on Ni(111); and CO_2 on PtNi(111), Generalized Gradient Approximation (GGA) along with the Perdew-Burke-Ernzerhof (PBE) functional was used. The local density approximation (LDA) and the Perwed Wang (PWC) functionals were used to obtain vibrational frequencies of CO, CO_2, CH_4, CH_3, CH_2 and CH on Ni(111) metal and on PtNi(111) surface alloy.

In analyzing the change in LDOS profiles of the surface metal atoms, Ni (or Pt), through which the adsorbate is bounded, and carbon atoms in their free and coordinated states, the nature of the site type was also considered. If adsorbate was adsorbed on an atop site, as the primary interaction is between the adsorbate and surface metal atom, the LDOS profiles of the coordinated atom of the adsorbate and surface metal atom on which the adsorption occurs were analyzed. However, if the adsorbate was adsorbed on a bridge site, the LDOS profiles of the coordinated atom of the adsorbate and one of the two surface metal atoms at the legs of the bridge site were analyzed. Therefore the change of LDOS profile of one of the surface metal atoms at the legs of the bridge site was considered as a result of 50% of adsorbate-adsorbent interaction due to the symmetry of adsorption system.

3.5.1. Parameters for Geometry Optimization

In the adsorption study of CO_2 on Ni(111) and PtNi(111), 2x3 supercell was used. The adsorption studies of CO and O on Ni(111) was conducted by using 2x2 supercell.

The quantum mechanical calculations at DMol3 tool box of Material Studio 6.0 were done with GGA-PBE functional by including the properties of DNP basis set and all electron relativistic – AER fundamentals. The size of the DNP basis set was 3.5.

In periodic DFT calculations, the variables to be adjusted are k-point set, cutoff energy, and vacuum thickness. K point sampling was used as 4x6x1 for 2x3 supercell, and

4x4x1 for 2x2 supercell. A 4.5 Å real space cut-off and 14 Å vacuum thickness were used in all geometry optimization calculations.

The vacuum thickness separates the metal atoms of the surface of interest and the bottom of the repeated slab. 14 Å of vacuum thickness was chosen to guarantee the elimination of possible interactions between those surfaces.

In the calculations, 5 layers thick slabs were built, including 2 bottom layers, whose atoms are fixed at their positions during the simulations and 3 top layers, whose atoms are allowed to move freely. The positions of the atoms at the bottom two layers were kept fixed in order to simplify the calculations and to decrease the simulation time. During the simulations, the adsorbate is also allowed to relax with the atoms of the top three layers of the adsorbent.

The tolerance of SCF convergence was $1x10^{-6}$. Fermi smearing was used as 0.001 hartree (Ha) (1 Ha=27.2114 eV) to improve the accuracy of DFT functional, GGA-PBE.

3.5.2. Parameters for Frequency Analysis

In the frequency analysis of CO_2, CO, O, CH_4, CH_3, CH_2 and CH on Ni(111) and PtNi(111), 2x2 supercell of Ni(111) and 2x3 supercell of PtNi(111) were used. At the upper surface of the PtNi(111) surface alloy, Pt concentration of 1/6 MLE (mono layer equivalent) was obtained by replacing one Ni surface atom per supercell with one Pt atom.

The quantum mechanical calculations at DMol3 tool box of Material Studio 6.0 were done with LDE-PWC functional by including the properties of DND basis set and all electron – AE fundamentals. The size of the DND basis set was 3.5 at the performed energy task of DMol3 tool box.

In periodic DFT calculations, k point samplings were used as 4x6x1 for 2x3 supercell, and 4x4x1 for 2x2 supercell. A 4.5 Å real space cut-off, 14 Å vacuum thickness were used in all frequency analysis calculations.

In the calculations, 5 layers thick slabs were built. The positions of the atoms at each layer were kept fixed in order to simplify the calculations and to decrease the simulation time.

The tolerance of SCF convergence was $1x10^{-5}$. Fermi smearing was used as 0.005 hartree (Ha) (1 Ha=27.2114 eV) to improve the accuracy of DFT functional, LDA-PWC.

4. RESULTS AND DISCUSSION

Dry reforming of methane involves two main reactions occurring simultaneously; methane dehydrogenation and CO_2 dissociation. The aim of this study is to investigate the adsorption properties of CO_2 and the products formed upon its dissociation, CO and O, on Ni(111) and PtNi(111) surfaces and forming a comparison basis to experimental FTIR-DRIFT studies through performing a frequency analysis of methane and its dehydrogenation products CH_3, CH_2, CH, and of CO_2, CO, O as the reactant and products of CO_2 dissociation reaction on Ni(111) an PtNi(111) surfaces via utilizing *ab initio* DMol3 tool box of Accelrys Material Studio.

Firstly adsorption behavior of all molecules that are involved in dissociation of CO_2 (CO_2, CO, O) on the catalytic surface were investigated. Preferred adsorption sites and adsorption energies were determined to understand how carbon dioxide dissociation occurs on Ni(111) surface. Adsorption of the products of CO_2 dissociation reaction on Ni(111) 2x2 supercell, and adsorption of CO_2 on Ni(111) and PtNi(111) 2x3 supercells were studied. PtNi(111) surface alloy was obtained by replacing one Ni atom on the surface of 2x3 Ni(111) supercell with one Pt atom; thus, the surface concentration of Pt on the upper layer of the Pt-Ni surface alloy was used as 1/6 MLE. Then, CO_2 adsorption energies, bond lengths and LDOS profiles are calculated for all possible adsorption sites of PtNi(111). Local Density of State analysis, which allows understanding the electronic interaction between the metal atoms of the sites and the adsorbate molecules, was also used whenever detailed analysis is necessary. After LDOS profiles of the adsorbate and adsorbent atoms involved in the adsorption process were obtained, the adsorption strength of the adsorbate molecules were evaluated and discussed on the basis of the calculated adsorption energies, bond lengths and adsorbate-adsorbent electronic interaction. Finally, frequencies of CO, CO_2, CH_4, CH_3, CH_2 and CH were determined on the possible adsorption sites of the Ni(111) and PtNi(111) surfaces by using the frequency calculation tool of DMol3 in order to form a comparison basis which will be used in the comparative analysis of stretching frequencies obtained from theoretical calculations on Ni(111) and PtNi(111) surfaces and

experimental results obtained through FTIR-DRIFT studies on Ni and Pt-Ni catalysts. The comparative analysis of calculated and experimental frequency data is expected to enable the determination of the catalytic sites of the Ni or PtNi catalysts that dominantly play roles in CDRM.

4.1. CO_2 Adsorption on Ni(111)

The adsorption of CO_2 at a constant surface coverage of 1/6 MLE, which guaranties insignificant adsorbate-adsorbate interaction, was analyzed on all possible adsorption sites. A single CO_2 molecule was placed on a (2×3) unit cell to simulate this surface coverage. CO_2 adsorption energies, C-O bond lengths and bond angles obtained for these four possible adsorption sites, i.e. atop, bridge, hollow hcp and hollow fcc shown in Figure 4.1, are reported in Table 4.1.

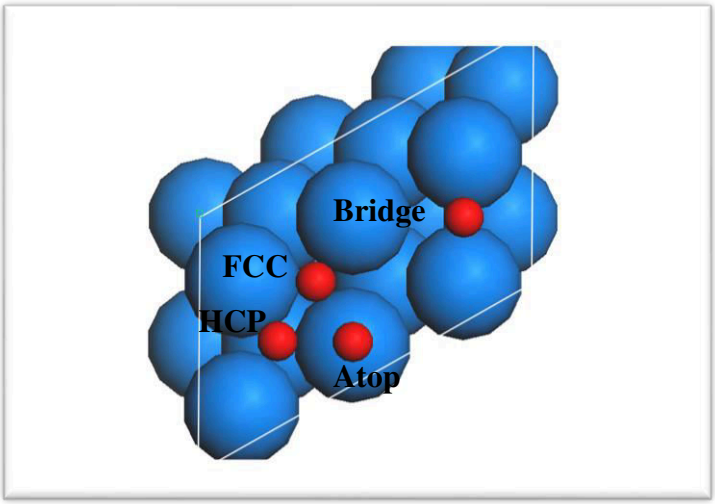

Figure 4.1. Ball model of Ni(111) surface and all adsorption sites studied in the geometry/energy optimization. Possible adsorption sites are specified with red balls and labeled as atop, bridge, hcp and fcc.

Even though the adsorption is an exothermic process, which leads negative adsorption energies, adsorption energies of CO_2 on Ni(111) surface were obtained extremely close to zero with positive values as given in Table 4.1. The reason of this special result for adsorption energies of CO_2 is that a significant portion of energy released during the adsorption process was spent for the configurational change of CO_2 molecule.

Free CO_2 has a linear configuration, but when CO_2 is adsorbed on Ni(111); the angle between two O atoms had been changed between 129^o and 134^o as listed in Table 4.1 and pictured in Figure 4.2, indicating a significant change in molecular geometry. Configuration change consumes the energy formed during the exothermic adsorption process. The important difference between LDOS profiles (Figure 4.5, Figure 4.6, Figure 4.7) of bare and coordinated C atom of CO_2 proves that there is a significant electronic interaction between CO_2 molecule and the surface confirming the occurrence of adsorption of CO_2 on Ni(111).

Table 4.1. Bond lengths between coordinated carbon of CO_2 and active Ni atom(s), carbon and first oxygen atoms of CO_2 and carbon and second oxygen atoms of CO_2 and bond angle and adsorption energy of CO_2 on all possible adsorption sites.

Adsorption Site	**Bond Length C-Ni (Å)**	**Bond Length C-O (Å)**	**Bond Length C-O (Å)**	**Bond Angle O-C-O (^{o})**	**Adsorption Energy (eV)**
Atop*	1.956	1.214	1.286	134.109	0.0968
Bridge	1.970-2.056	1.278	1.279	131.889	0.1530
Hollow FCC*	1.940-2.360-2.228	1.275	1.274	129.389	0.2086
Hollow HCP*	1.918-2.181-2.572	1.275	1.275	131.477	0.1528

* Geometry optimized CO_2 molecule left its original adsorption site and moved to the bridge site of Ni(111) surface.

The stable adsorption site could be defined as the site at which CO_2 is bound with the minimum adsorption energy. But, because of the special adsorption process that occurs simultaneously with configurational change, considering only the adsorption energy to decide whether the adsorption is stable may be misleading. In order to decide whether the adsorption is stable or not; geometry of the energy optimized system along with the LDOS profiles of both coordinated metal atom and the coordinated atom of the adsorbate molecule were used. When original and energy optimized configurations are compared

with each other, it is seen that CO_2 adsorption on bridge site is stable. CO_2 on atop, fcc and hcp sites slightly moves through the bridge site as seen in Figure 4.3 and 4.4. Bridge site is also mentioned as the stable adsorption site of CO_2 on Ni(111) surface in the study of *Wang et al., 2007*.

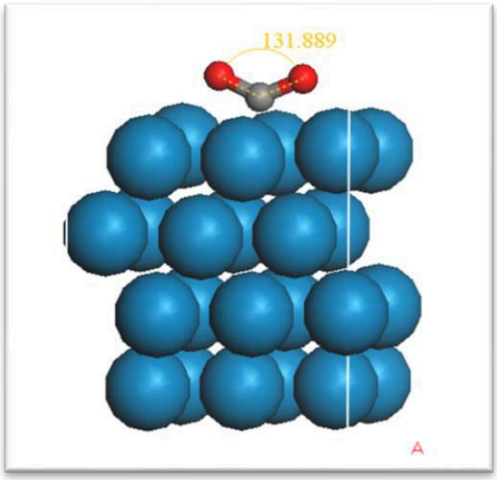

Figure 4.2. Geometry/energy optimized configuration of CO_2 molecule that was originally placed at bridge adsorption site of Ni(111).

The orbital of bare CO_2 which interact particularly with the metal d bands produce peaks below the Fermi level. The highest occupied molecular orbital (HOMO) of free CO_2 is $1\pi_g$ and the lowest unoccupied molecular orbital (LUMO) of it is $2\pi_\mu$. LUMO is situated at 0.15 Ha and HOMO is situated at 0.23 Ha in the LDOS profile of free CO_2. (Choe *et al.,* 2001, Gautam *et al.,* 2013) Upon adsorption, $2\pi_\mu$ band was divided into two peaks by downward shifts with decreasing amplitude, and π_g band was downward shifted as a single peak with a decreasing amplitude for geometry optimized CO_2 at all possible adsorption sites on Ni(111) surface. In other words, there was a significant decrease in electron density around the coordinated carbon of the CO_2 in the corresponding energy levels upon adsorptions on all sites. LDOS profiles of the C of bare and geometry optimized CO_2, which was placed at atop, bridge and hcp adsorption sites originally, can be seen in Figures 4.4, 4.6 and 4.7. Simultaneously, electron density of the active Ni atom that is involved in adsorption, ie. Ni on which C is bound, increases in 0 – (-0.2) Ha energy range for all adsorption configurations. The LDOS profile of geometry optimized Ni atom was shown

for fcc adsorption site in Figure 4.8 as an example. The decrease in electron density of carbon and increase in electron density of active Ni prove that there is a significant electronic interaction between Ni and CO_2, and the adsorption is occurred between the CO_2 and the active Ni atom at all possible adsorption sites. It must be noted that, stable CO_2 adsorption site on Ni(111) upon geometry optimization is found as bridge site regardless of the initial CO_2 position prior to the simulation.

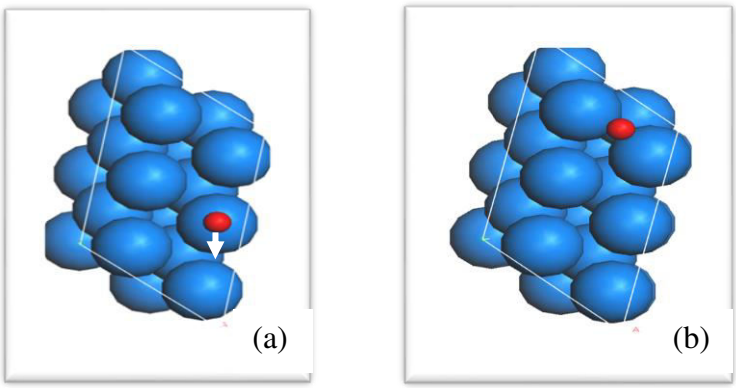

Figure 4.3. CO_2 adsorption on atop and bridge sites of Ni(111). (a) Original configuration of CO_2 at atop site is specified with a red ball and slight movement of geometry/energy optimized CO_2 to the bridge site from atop site is shown with an arrow, (b) original configuration of CO_2 at bridge site is specified with a red ball, and it is stable at the same configuration after geometry/energy optimization.

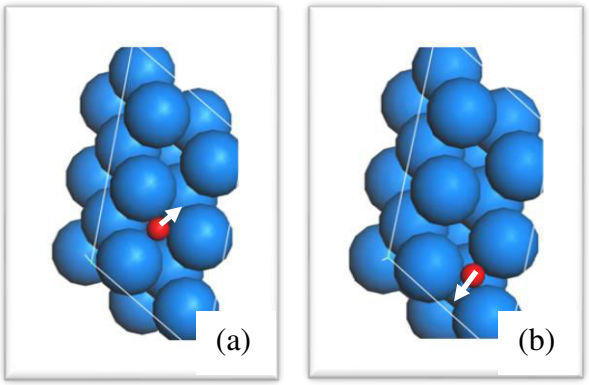

Figure 4.4. Multifold CO_2 adsorption on Ni(111). (a) Original configuration of CO_2 at FCC site is specified with a red ball and slight movement of geometry/energy optimized CO_2 to the bridge site from FCC site is shown with an arrow, (b) original configuration of CO_2 at HCP site is specified with a red ball and slight movement of geometry/energy optimized CO_2 to the bridge site from HCP site is shown with an arrow.

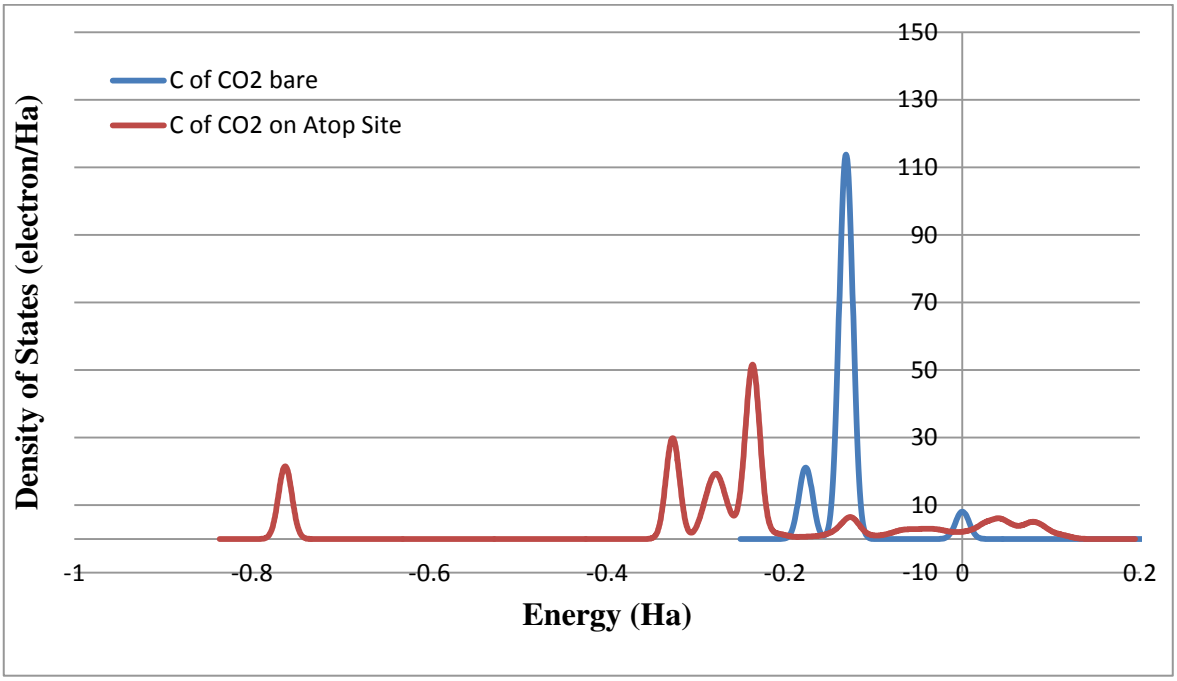

Figure 4.5. Changes in LDOS profile of C of geometry optimized CO_2 molecule that was originally placed at atop adsorption site compared to that of the C of bare CO_2 molecule.

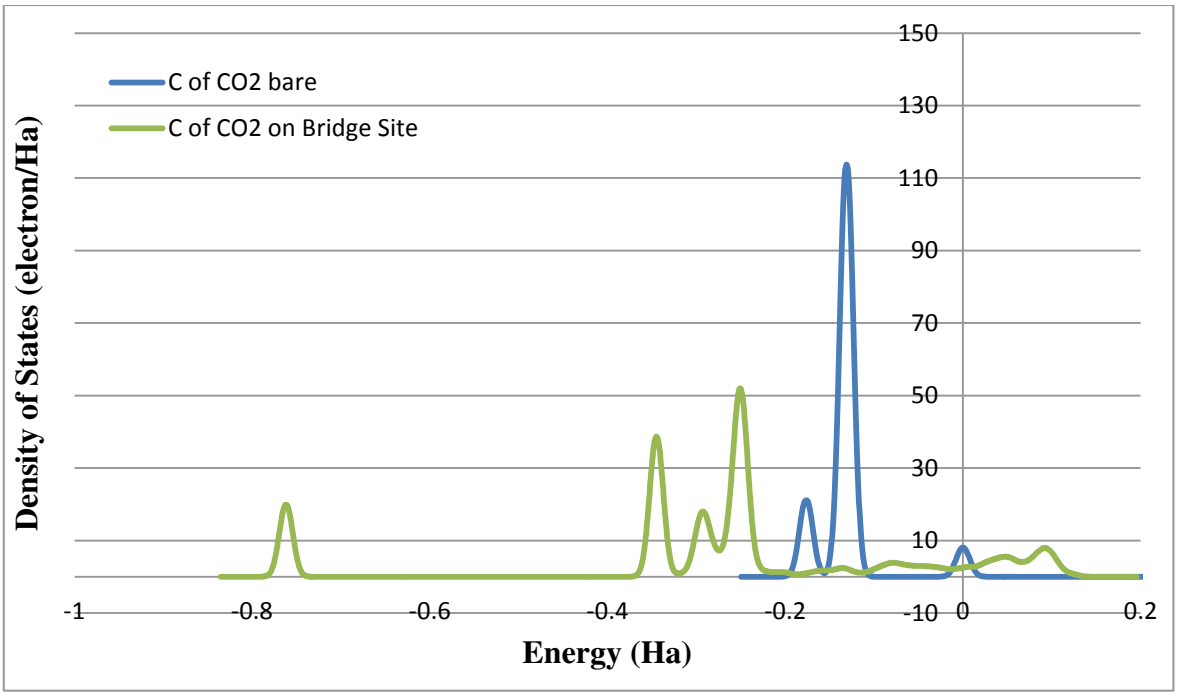

Figure 4.6. Changes in LDOS profile of C of geometry optimized CO_2 molecule that was originally placed at bridge adsorption site compared to that of the C of bare CO_2 molecule.

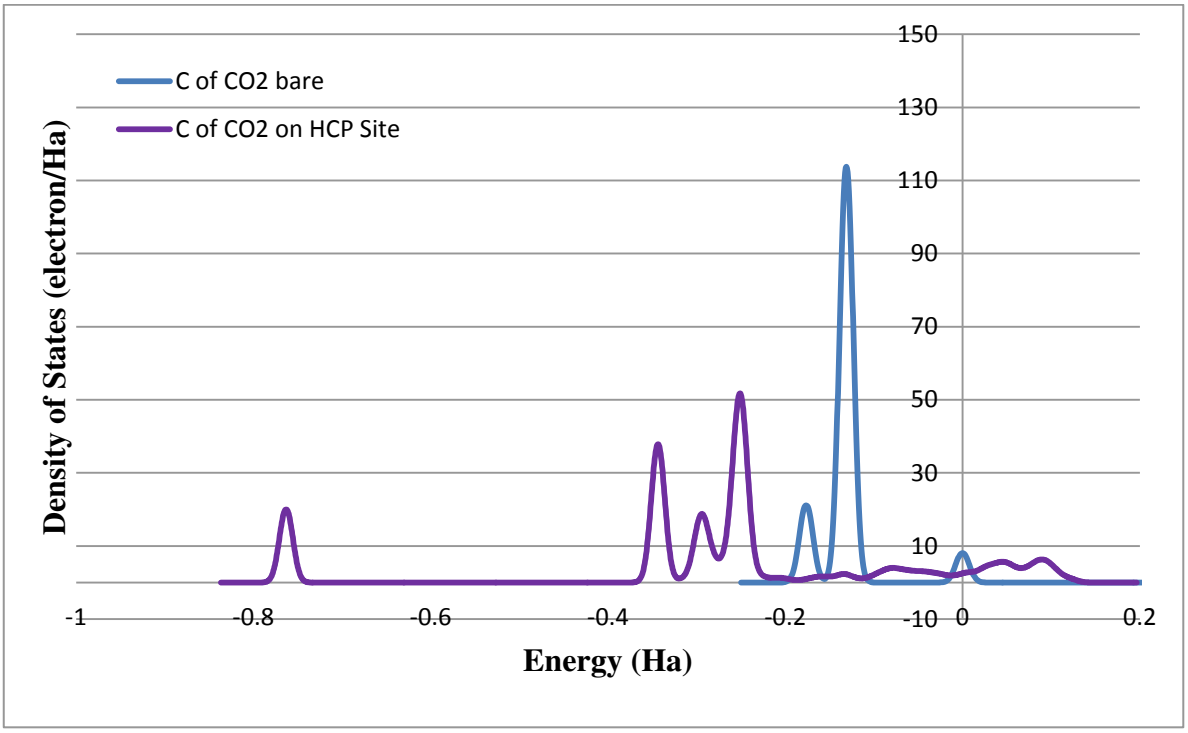

Figure 4.7. Changes in LDOS profile of C of geometry optimized CO_2 molecule that was originally placed at hcp adsorption site compared to that of the C of bare CO_2 molecule.

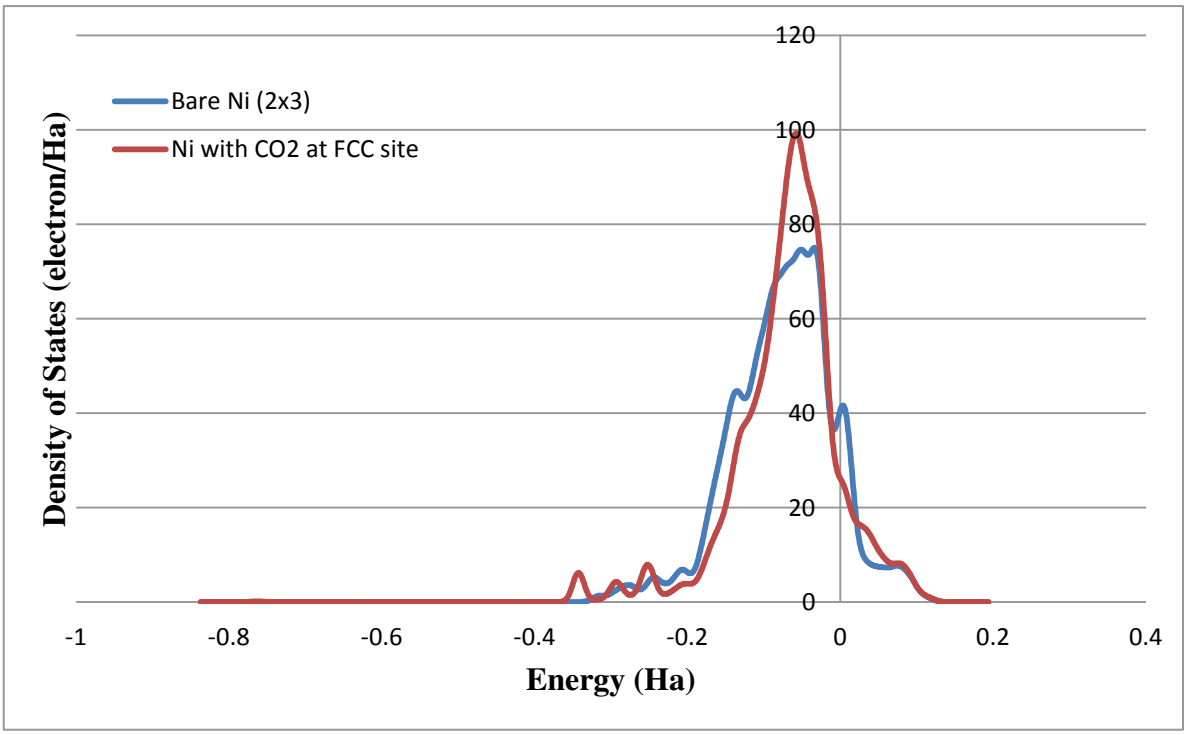

Figure 4.8. Changes in LDOS profile of CO_2-coordinated Ni at the fcc site upon geometry optimization compared to that of the bare Ni.

4.2. CO_2 Adsorption on PtNi(111) Surface Alloy

CO_2 adsorption at a constant surface coverage of 1/6 MLE, which guaranties insignificant adsorbate-adsorbate interaction, was analyzed on all possible adsorption sites; atop, bridge and threefold positions on PtNi(111) surface alloy. One of the six Ni atoms present on upper surface of Ni(111) 2x3 unit cell was replaced by one Pt atom to build PtNi(111) surface alloy. A single CO_2 molecule was placed on a (2×3) unit cell to simulate surface coverage of 1/6 MLE (Figure 4.9).

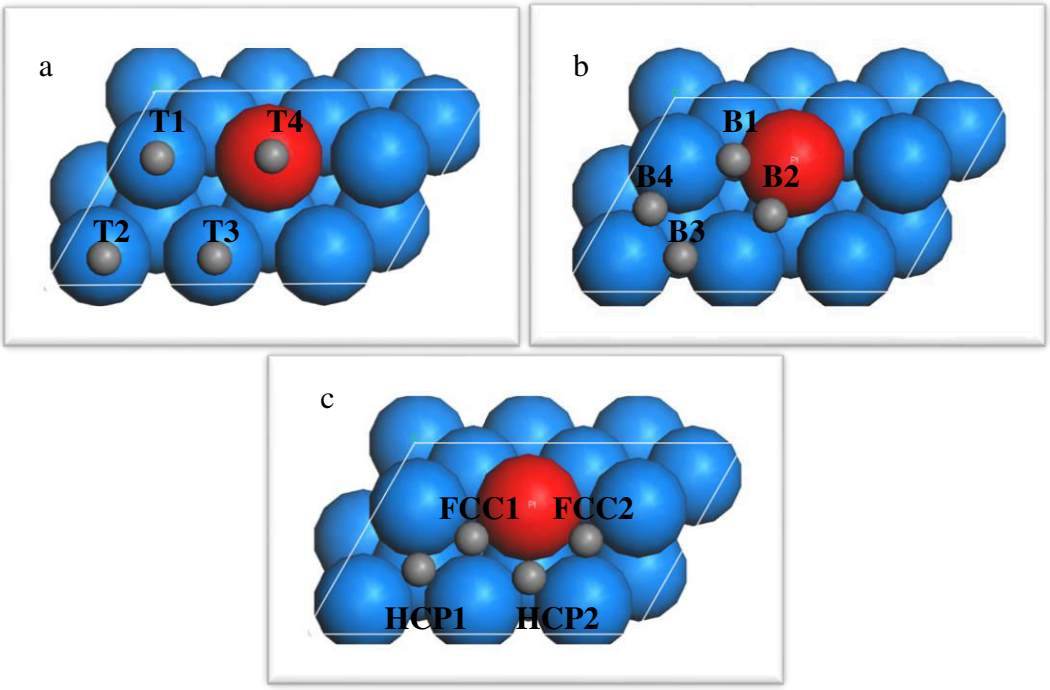

Figure 4.9. Ball model of PtNi(111) surface alloy and all adsorption sites studied in the geometry/energy optimization. The balls in red and blue color represent Pt and Ni atoms, respectively. Possible adsorption sites are pointed with grey balls and labeled as T1, T2, T3, T4 for atop adsorption sites in Figure 4.9a; B1, B2, B3, B4 for bridge adsorption sites in Figure 4.9b; FCC1, FCC2, HCP1, HCP2 for threefold adsorption sites in Figure 4.9c.

CO_2 molecules that were placed on different possible atop adsorption sites called as T1, T2, T3 and T4. Figure 4.9.a describes the original positions of CO_2 on possible atop adsorption sites. The binding leg of CO_2 at T4 is Pt, while for the other atop adsorption sites the binding leg is Ni. CO_2 molecules that were originally placed on atop adsorption

sites were found not stable on their original configurations. The CO_2 molecules originally placed at atop sites were diffused to and stabilized at the bridge sites in their closest neighborhood upon geometry optimization (Figure 4.10). Those bridge sites have both binding legs on Ni atoms for CO_2 molecules that was originally placed on T1, T2, T3, and one leg on Pt atom and one leg on Ni atom for CO_2 molecule that was originally placed on T4.

CO_2 molecule that was placed originally on all possible bridge adsorption sites, which are called as B1, B2, B3 and B4, are shown in Figure 4.9.b. The binding legs of original adsorption sites of B1 and B2 are one Pt atom and one Ni atom, whereas for B3 and B4, the original adsorption sites have both binding legs on Ni atoms. CO_2 molecules that were originally placed on bridge adsorption sites are stable at their original configurations except the CO_2 molecule which was placed originally on B3; that molecule was flown away from the PtNi(111) surface with a linear molecular structure upon geometry optimization indicating insignificant interaction with the adsorbate surface resulting desorption.

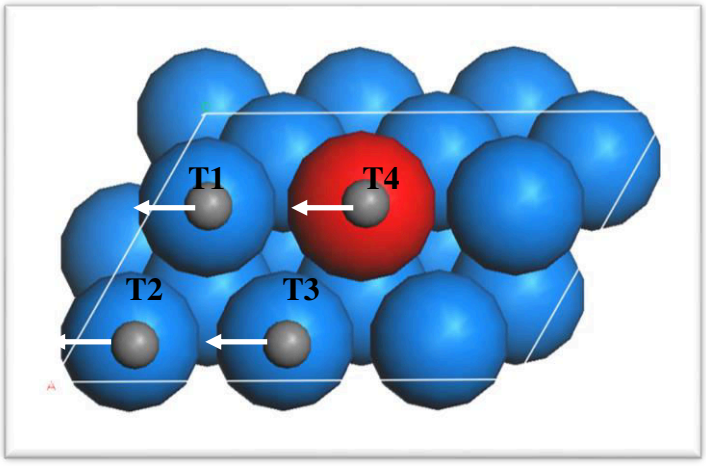

Figure 4.10. Diffusion directions of originally atop-bound CO_2 molecules to the bridge adsorption sites upon geometry/energy optimization are on PtNi(111). The balls in red and blue color represent Pt atoms and Ni atoms, respectively. Grey balls represent CO_2 molecules.

CO_2 molecule that was placed originally on several possible threefold adsorption sites are called as FCC1, FCC2, HCP1 and HCP2 (Figure 4.9.c). Hollow fcc and hollow hcp orginal adsorption sites, FCC1 and HCP2, have one binding leg on Pt atom and two binding legs on Ni atoms. FCC2 and HCP1 original adsorption sites have all three binding legs on Ni atoms. CO_2 molecules that were originally placed on threefold adsorption sites were not stable on their original configurations and have tendency to diffuse and stabilize at the bridge sites (Figure 4.11). Geometry optimized CO_2 molecules originally placed at FCC1, FCC2 and HCP2 diffused to and stabilized at bridge sites having one binding leg on Ni atom and the other on Pt atom, whereas both binding legs of CO_2 which was originally placed at HCP1 are on Ni atoms at the bridge site where it is stabilized.

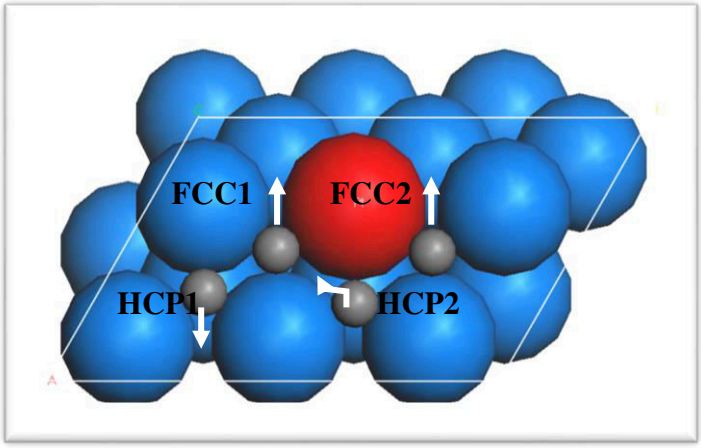

Figure 4.11. Diffusion directions of CO_2 molecules placed original at threefold adsorption sites. Upon geometry optimization, the molecules are diffused to and stabilized at the bridge adsorption sites of PtNi(111). The balls in red and blue color represent Pt atoms and Ni atoms, respectively. Grey balls represent CO_2 molecules.

As mentioned in the Section 4.1 adsorption on metal surfaces is an exothermic process which leads negative adsorption energies. Adsorption energies of CO_2 on PtNi(111) surface alloy were obtained extremely close to zero, with positive and negative values, as given in Table 4.2. The reason of this special result is that a significant portion of the energy released through the interaction with the surface was spent for the configurational change of CO_2 molecule during adsorption process; if there is a significant electronic interaction between the CO_2 molecule and the surface, CO_2 molecule, which

has a linear geometry in its free form, assumes a bent geometry upon energy optimization. In this study, when CO_2 is adsorbed on PtNi(111) surface alloy; the O-C-O angle had been calculated as between 129^o and 135^o (Table 4.2); the geometry of a representative CO_2 molecule upon optimization is pictured in Figure 4.12. The significant difference between LDOS profiles (Figure 4.14, Figure 4.16, Figure 4.18 and Figure 4.19) of free and coordinated C atom of CO_2 proves that there is a significant electronic interaction between CO_2 molecule and the surface.

When CO_2 molecules are originally placed at T3 and B3, their geometry optimized structures upon adsorption are linear, indicating the absence of interaction between CO_2 and the surface. Upon energy optimization, the CO_2 molecules were away from the surface indicating desorption, which also verifies the absence of interaction between adsorbate and adsorbent, as can be seen in Table 4.2.

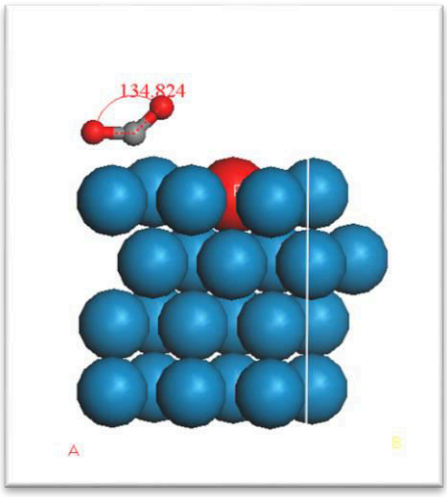

Figure 4.12. Geometry optimized configuration of CO_2 molecule that was originally placed at adsorption site T1 of PtNi(111) surface alloy.

The strongest interaction between adsorbate and adsorbent was observed when the original adsorption site is B1. The CO_2 molecule was positioned significantly close the surface upon optimization. One of the CO bonds was elongated and its oxygen atom was moved away from surface, as seen in Figure 4.13. There was a great structural change in the molecule; hence, the geometry optimization of DMol3 tool box stopped calculations

without ending them. This is a computational limitation and the reason why the adsorption energy could not be obtained for original adsorption site B1.

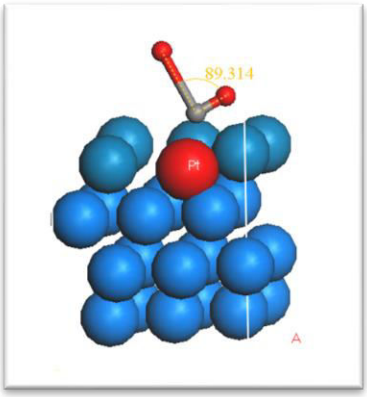

Figure 4.13. Geometry optimized configuration of CO_2 molecule that was originally placed at adsorption site B1 of PtNi(111) surface alloy.

As mentioned in Section 4.1, adsorption of CO_2 on an adsorption site is called strong and stable when CO_2 is bound with minimum adsorption energy. But, as the adsorption process occurs simultaneously with configurational change of the adsorbate CO_2, considering only the adsorption energy to decide whether the adsorption is stable may be misleading. In order to decide whether the CO_2 adsorption on the site is stable, the geometry of the energy optimized system as well as the changes in the LDOS profiles of coordinated atoms at the adsorbent surface and the adsorbate molecule, compared to their uncoordinated states, should be considered. When original and energy optimized configurations are compared with each other, the CO_2 adsorption on bridge sites B1, B2, B3 and B4 are found stable.

Table 4.2. Bond lengths between coordinated carbon of CO_2 and active Ni atom(s) and/or Pt atom, carbon and first oxygen atoms of CO_2, carbon and second oxygen atoms of CO_2 and bond angle and adsorption energy of CO_2 on all possible adsorption sites.

Adsorption Side	**Bond Length C-Ni/Pt (Å)**	**Bond Length C-O (Å)**	**Bond Length C-O (Å)**	**Bond Angle O-C-O (^{o})**	**Adsorption Energy (eV)**
T1*	1.957	1.283	1.211	134.824	0.2405
T2*	1.974	1.282	1.211	135.342	0.2524

Table 4.2. Bond lengths between coordinated carbon of CO_2 and active Ni atom(s) and/or Pt atom, carbon and first oxygen atoms of CO_2, carbon and second oxygen atoms of CO_2 and bond angle and adsorption energy of CO_2 on all possible adsorption sites (cont.).

Adsorption Side	**Bond Length C-Ni/Pt (Å)**	**Bond Length C-O (Å)**	**Bond Length C-O (Å)**	**Bond Angle O-C-O (^{o})**	**Adsorption Energy (eV)**
T3*^{o}	3.662	1.175	1.175	180	-0.0654
T4*	2.095	1.211	1.201	132.419	-0.0103
B1$^/$	2.196-2.360	2.714	1.309	89.314	-
B2	2.105-3.065	1.21	1.294	132.823	0.0418
B3^o	3.863-3.710	1.177	1.176	180	-0.0647
B4	2.108-1.985	1.281	1.259	132.540	0.3822
FCC1*	2.601-2.095-3.062	1.211	1.293	132.434	-0.0099
FCC2*	2.621-2.089-3.016	1.211	1.296	132.333	0.0131
HCP1*	1.969-2.232-2.306	1.268	1.263	131.067	0.5344
HCP2*	1.969-2.232-2.306	1.268	1.263	129.635	0.3258

* Geometry optimized CO_2 molecule left its original adsorption site and moved to the closest bridge site of PtNi(111) surface, like shown in the Figure 4.10.

^{o} CO_2 molecule keeps its linearity at the geometry optimized configuration on PtNi(111) surface alloy.

$^/$ One of the O atoms of CO_2 molecule was separated from the CO_2 molecular structure at the geometry optimized configuration on PtNi(111) surface alloy.

As mentioned in Section 4.1, the molecular orbitals of bare CO_2, which interact particularly with the metal d bands during adsorption, produce peaks below the Fermi level. The highest occupied molecular orbital (HOMO) of free CO_2 is $1\pi_g$ and the lowest unoccupied molecular orbital (LUMO) of it is $2\pi_\mu$. LUMO is situated at 0.15 Ha and HOMO is situated at 0.23 Ha in the LDOS profile of the C of free CO_2 (Choe *et al.,* 2001, Gautam *et al.,* 2013). Upon adsorption, $2\pi_\mu$ band was divided into two peaks along with the downward shift with decreasing amplitude, and π_g band was downward shifted as a

single peak with a decreasing amplitude for geometry optimized CO_2 at all possible adsorption sites on PtNi(111) surface alloy except when T3 and B3 was chosen as the original adsorption sites. In other words, there is a significant decrease in electron density around carbon in the corresponding energy levels when there is a significant adsorbate-adsorbent interaction yielding adsorption. Comparative analysis of the LDOS profiles of geometry optimized forms of the C of CO_2 molecule at the adsorption site, which was originally placed at atop, bridge and threefold adsorption sites, and that of free CO_2 can be seen in Figures 4.14, 4.16, 4.18 and 4.19.

LDOS profiles of C of CO_2 molecules, which were originally placed at adsorption sites T3 and B3, (Figure 4.15 and Figure 4.17) verifies weak adsorption of CO_2 molecule on PtNi(111) surface alloy. $2\pi_\mu$ and π_g bands were shifted downward only with slightly decreasing amplitudes.

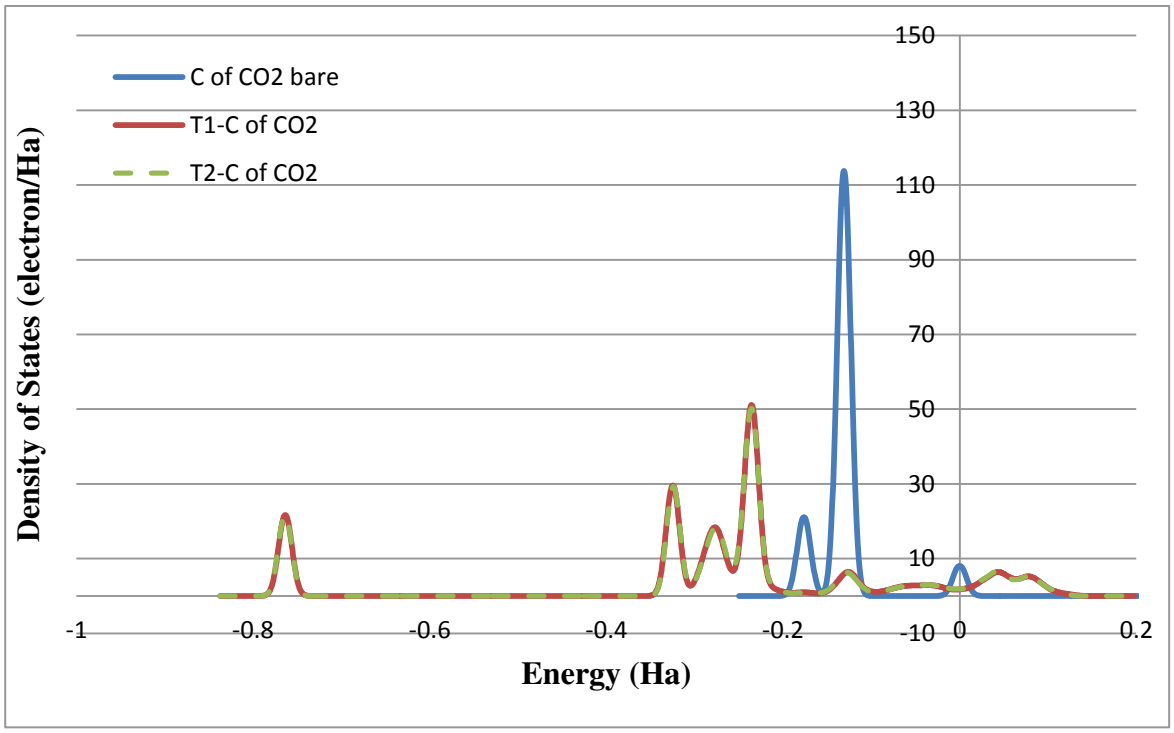

Figure 4.14. Changes in LDOS profile of C of geometry optimized CO_2 molecule that was originally placed at T1 and T2 adsorption sites compared to that of C of bare CO_2 molecule.

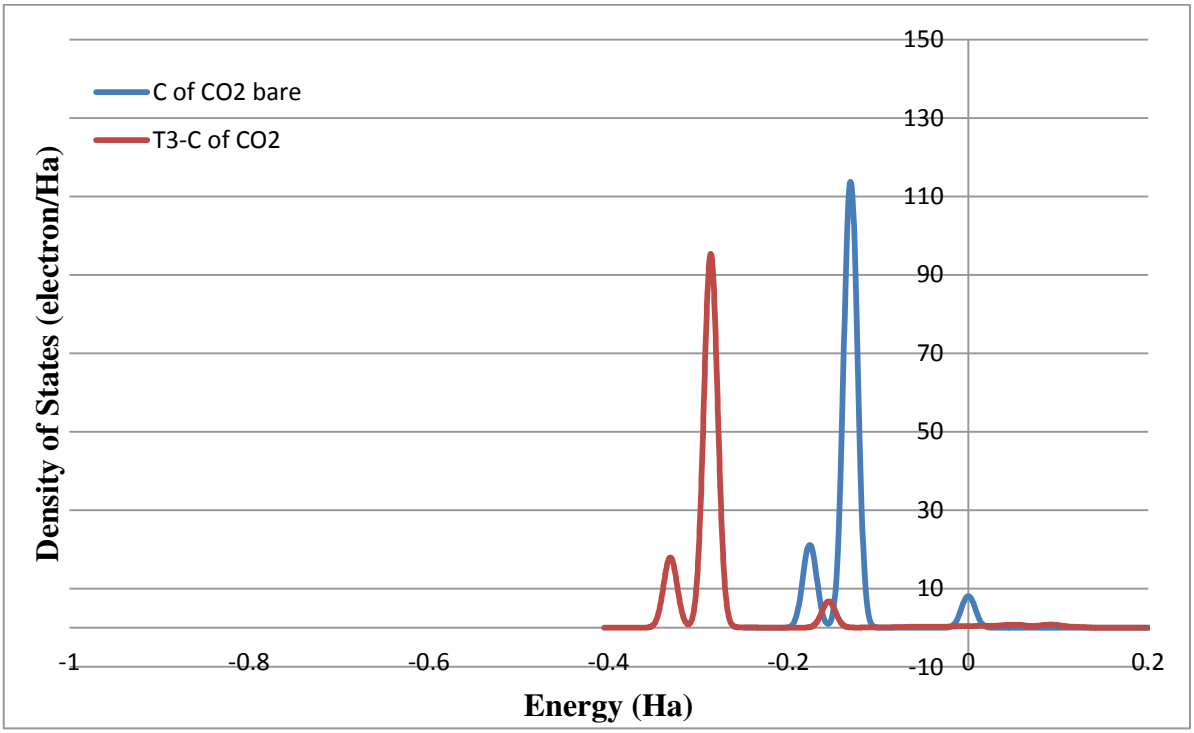

Figure 4.15. Changes in LDOS profile of C of geometry optimized CO_2 molecule that was originally placed at T3 adsorption sites compared to that of C of bare CO_2 molecule.

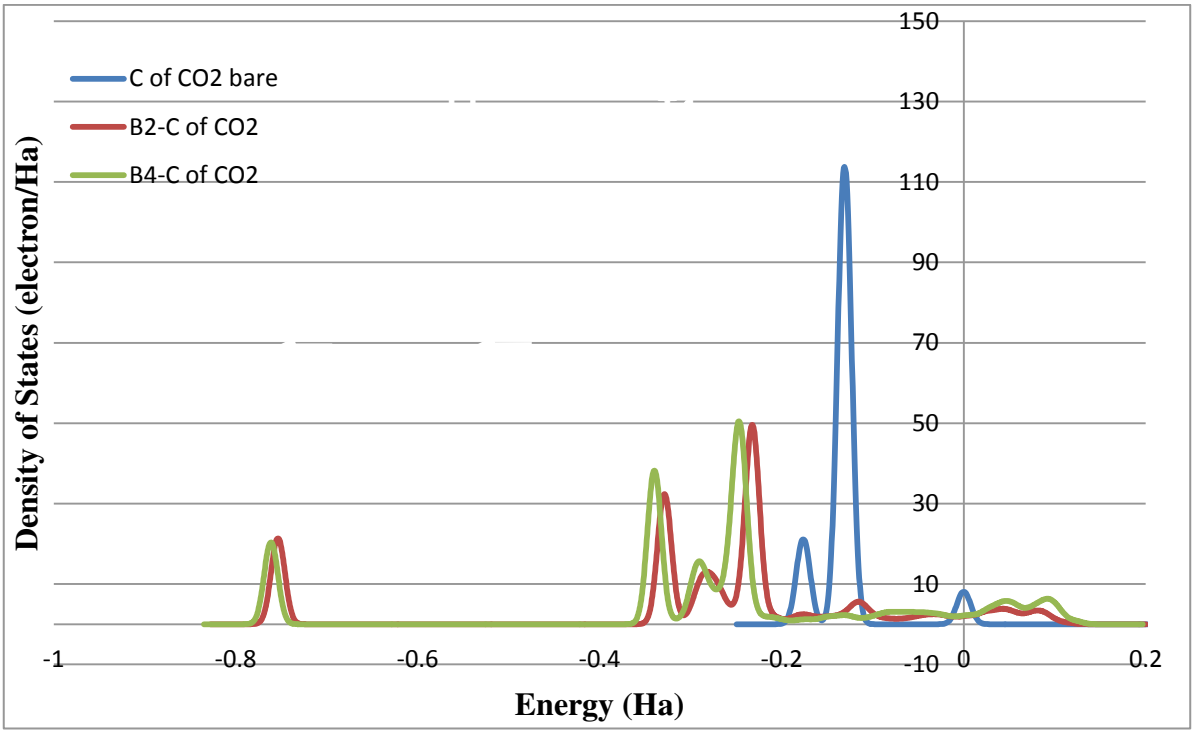

Figure 4.16. Changes in LDOS profile of C of geometry optimized CO_2 molecule that was originally placed at B2 and B4 adsorption sites compared to that of C of bare CO_2 molecule.

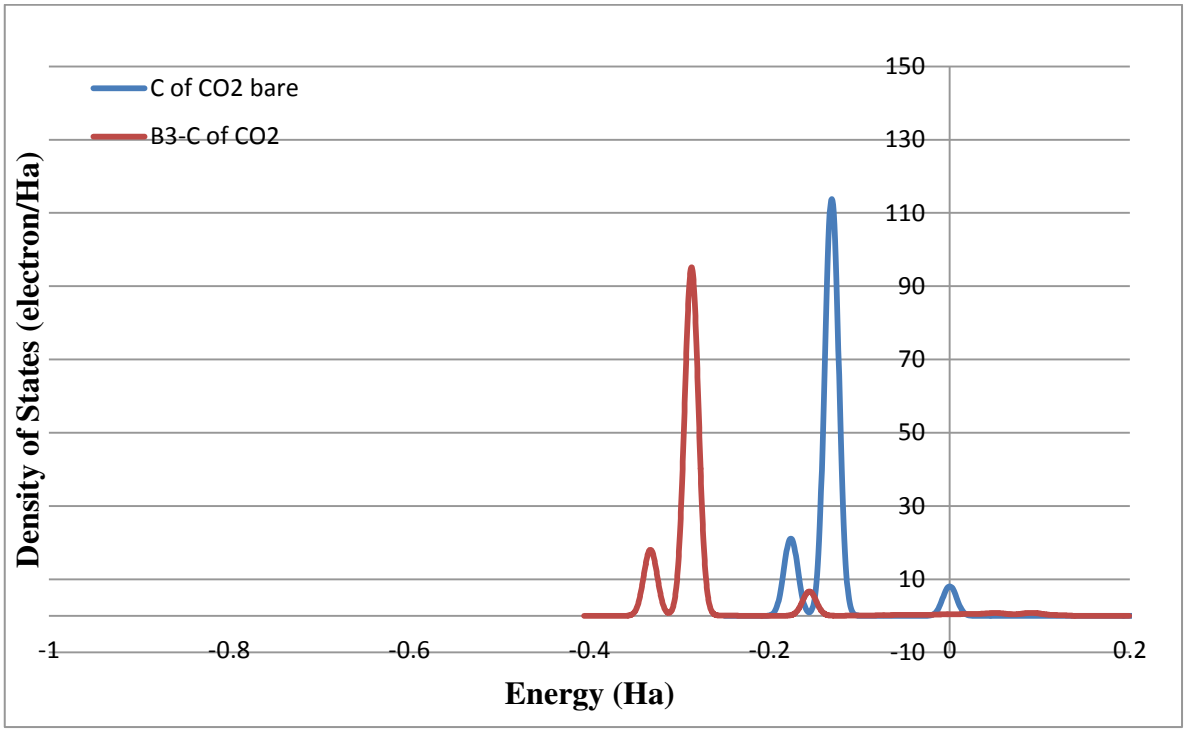

Figure 4.17. Changes in LDOS profile of C of geometry optimized CO_2 molecule that was originally placed at B3 adsorption sites compared to that of C of bare CO_2 molecule.

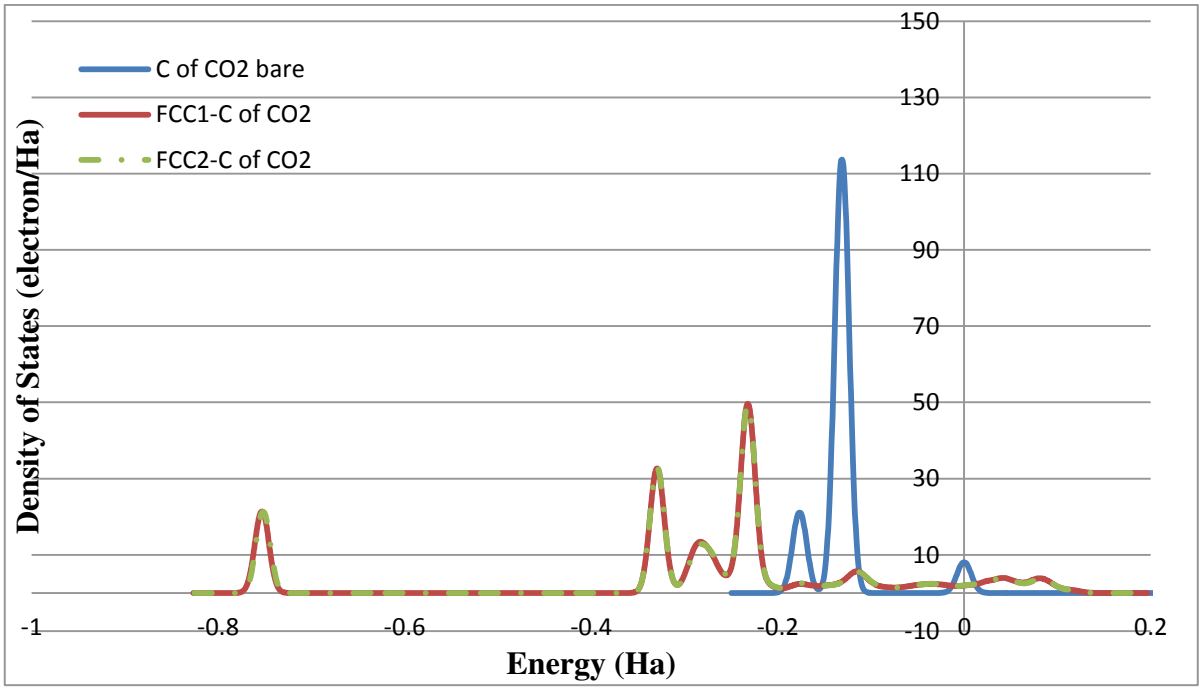

Figure 4.18. Changes in LDOS profile of C of geometry optimized CO_2 molecule that was originally placed at FCC1 and FCC2 adsorption sites compared to that of C of bare CO_2 molecule.

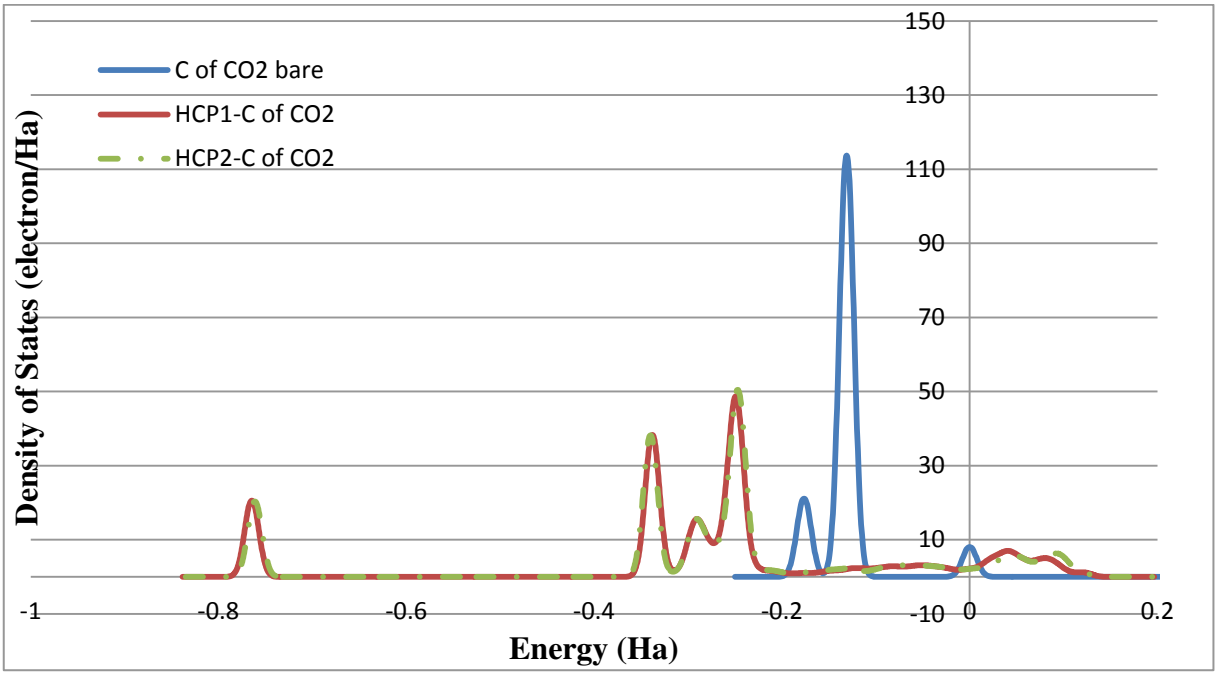

Figure 4.19. Changes in LDOS profile of C of geometry optimized CO_2 molecule that was originally placed at HCP1 and HCP2 adsorption sites compared to that of C of bare CO_2 molecule.

4.3. CO Adsorption on Ni(111)

CO adsorption at a constant surface coverage of 1/4 MLE was analyzed for all possible atop, bridge and threefold adsorption sites of Ni(111) surface. A single CO molecule was placed on a (2×2) unit cell surface to simulate the surface coverage of 1/4 MLE (Figure 4.20). The CO adsorption energies on atop, bridge, hollow hcp and hollow fcc adsorption sites are reported in Table 4.3.

As mentioned in the Section 4.1 and 4.2, adsorption is an exothermic process which leads negative adsorption energies for adsorbate molecule on the metal surface. Adsorption energies of CO on Ni(111) surface were obtained as negative values as expected theoretically. The adsorption energy values (Table 4.3) prove that CO adsorption was strong on all adsorption sites of Ni(111) surface. The study of *Orita et al., 2004* also confirms the strong interaction between CO and Ni(111) surface accompanied by chemisorption process. The strongest chemisorption was observed at HCP site with

-1.9087 eV of adsorption energy. The geometry of the energy optimized CO molecules on the adsorption site confirms that CO adsorption was stable at the original positions.

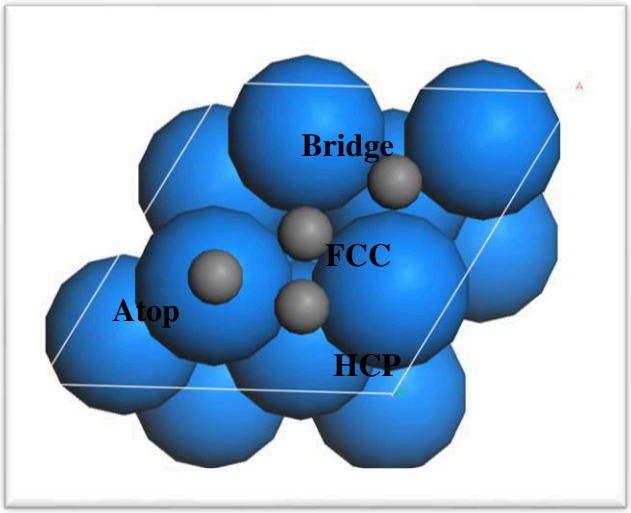

Figure 4.20. Ball model of Ni(111) surface and all adsorption sites studied in the geometry/energy optimization. The balls in blue color represent Ni atom. Possible adsorption sites are shown by grey balls and labeled as Atop, Bridge, FCC and HCP.

Table 4.3. Bond lengths between (i) coordinated carbon and active Ni atom(s), (ii) carbon and oxygen atoms of CO, and adsorption energy of CO on all possible adsorption sites.

Adsorption Side	**Bond Length C-Ni (Å)**	**Bond Length C-O (Å)**	**Adsorption Energy (eV)**
Atop	1.745	1.163	-1.5224
Bridge	1.872-1.894	1.183	-1.6901
HCP	1.952-1.954-1.961	1.191	-1.9087
FCC	1.942-1.955-1.982	1.191	-1.7722

4.4. O Adsorption on Ni(111)

The adsorption of oxygen at a constant surface coverage of 1/4 MLE was analyzed on all possible atop, bridge and threefold adsorption sites of Ni(111). A single O molecule

was placed on a (2×2) unit cell to simulate the surface coverage of 1/4 MLE (Figure 4.20). Oxygen adsorption energies on atop, bridge, hollow hcp and hollow fcc adsorption sites are reported in Table 4.4.

Table 4.4. Bond lengths between coordinated oxygen and surface atom(s), and adsorption energy of oxygen on each site.

Adsorption Side	**Bond Length O-Ni (Å)**	**Adsorption Energy (eV)**
Atop*	1.842	-5.7981
Bridge*	1.841-1.842	-5.5953
HCP	1.844-1.843-1.842	-5.7981
FCC	1.840-1.843-1.843	-5.7979

* Geometry optimized O molecule left its original adsorption site and moved to the hollow sites of 2x2 unit cell of Ni(111) surface.

Adsorption energies of O on Ni(111) surface were obtained as negative values, as expected theoretically. The adsorption energies listed in Table 4.4 prove that the adsorption was strong at each adsorption site on Ni(111) surface. The study of *Das and Shoji, 2011*, also confirms the above mentioned strong interaction yielding strong O adsorption on Ni(111) surface. Oxygen atom initially placed at hcp and fcc sites are stable at their original positions upon energy optimization. On the other hand, oxygen atom placed originally on atop and bridge sites moved to neighboring hollow sites.

4.5. Frequency Analysis of CO, CO_2, CH_4, CH_3, CH_2 and CH

Frequency analysis of molecules CO, CO_2, CH_4, CH_3, CH_2 and CH on monometallic Ni (111) surface and PtNi(111) surface alloy for all possible adsorption sites were made through the use of LDA-PWC functionals of DMol3 tool box aiming to form a reference data base to be compared with the result of experimental FTIR-DRIFT studies conducted over Ni/Al_2O_3 and $Pt\text{-}Ni/Al_2O_3$ catalysts under the atmosphere containing

CO,CO_2 and CH_4 or their combination. It should be noted that in frequency analysis the optimized geometries previously calculated with GGA-PBE are not considered as the initial configuration of the system. In this section all the calculations were performed again by using LDA-PWC functional, which is preferred for identifying stretching frequencies for those complex systems. For the monometallic surface, effect of adsorbate surface concentration on the stretching frequency of the adsorbate is also considered; the frequency analysis on Ni(111) surface was performed on 2x2 supercell with 1/2 MLE and 1/4 MLE adsorbate molecule concentrations. Frequency analysis on PtNi(111) surface was performed on 2x3 supercell with 1/6 MLE adsorbate molecule concentration. The adsorption sites used for Ni(111) and PtNi(111) surfaces in the frequency analysis are shown in Figure 4.21 and 4.22, respectively.

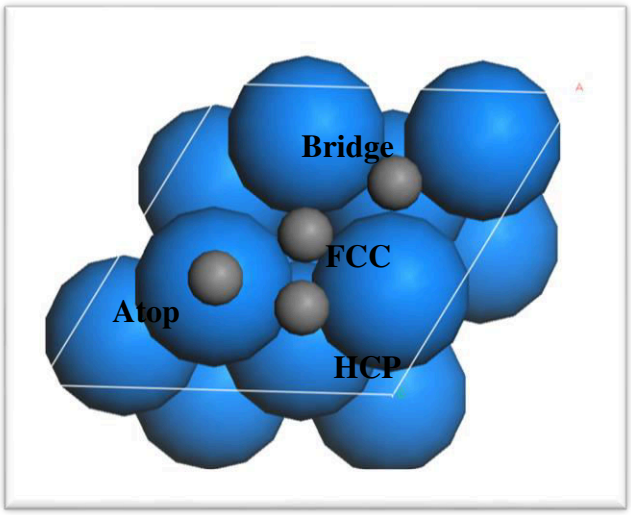

Figure 4.21. Ball model of Ni(111) surface and all adsorption sites studied in the frequency analysis. The balls in blue color represent Ni atom. Possible adsorption sites are shown by grey balls and labeled as Atop, Bridge, FCC and HCP.

Calculated stretching frequencies for each adsorbed molecule on each adsorption site are listed in Table 4.5, Table 4.6 and Table 4.7. Five of the frequency results could not be calculated in DMol3 tool box by using LDA-PWC functionals because of the significant geometry change of the adsorbate molecule, which leads termination of the simulation.

As explained in Section 2.3 in detail, CO vibrational frequency is given between 2060-1907 cm^{-1} band on Ni metal surface and 2079-2064 cm^{-1} on PtNi surface alloy in the literature. The C–H stretching frequency on Ni metal was found to be 2965 and 2970 cm^{-1} experimentally. As a general evaluation of the results, this band ranges are compatible with the calculated stretching frequencies reported in this study. Experimental and theoretical works confirm that stretching frequency of the adsorbed molecule on the surface shows differences according to the temperature and surface coverage. (Diaguez *et al.,* 2010a, Vannice, 1982, Schilbe et al., 1995, Yoshinobu and Kawai, 1996, Formonso et al., 2006, Watwe et al., 2000, Yang and Whitten, 1996).

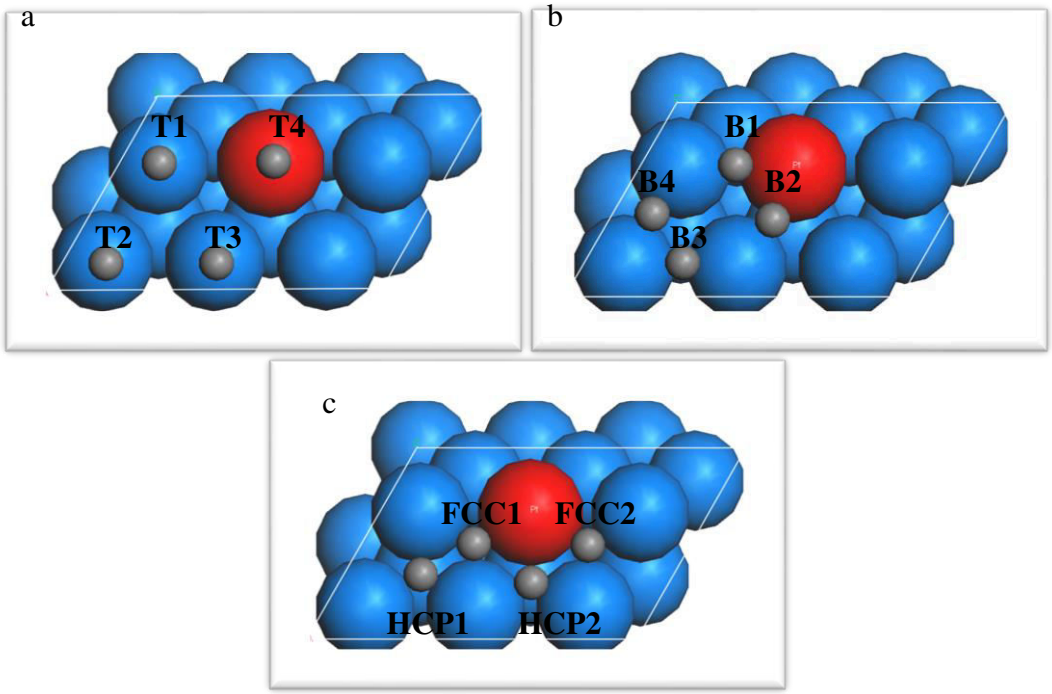

Figure 4.22. Ball model of PtNi(111) surface alloy and all adsorption sites studied in the frequency analysis. The balls in red and blue color represent Pt atoms and Ni atoms, respectively. Possible adsorption sites are shown by grey balls and labeled as T1, T2, T3, T4 for atop adsorption sites in Figure 4.22a; B1, B2, B3, B4 for bridge adsorption sites in Figure 4.22b; FCC1, FCC2, HCP1, HCP2 for threefold adsorption sites in Figure 4.22c.

It is reported that the frequency of the CO molecule adsorbed on Ni metal surface increases with a decrease in temperature. Peaks of the IR spectrum were obtained at 2017 and 1097 cm^{-1} at room temperature and at 2184 and 2167 cm^{-1} at low temperature (Diegues

et al., 2010a). In the study of *Vannice,* predominant band is shifting from 1830 to 1900 cm^{-1} at low coverage. Same phenomena (i.e. increasing frequency in response to the decrease in coverage) for adsorbate CO on Ni metal surface is also confirmed by the results of the current study (Table 4.5).

CO stretching frequencies calculated (Table 4.5) for 1/2 MLE showed that the frequency is 2099 cm^{-1} for atop adsorption and shifted to 1971-1987 cm^{-1} band range when the adsorption type is changed to bridge or multifold adsorption. As the concentration decreased to 1/4 MLE, either a limited increase in stretching frequency, as in atop and bridge type, or no change, as in multifold type adsorption, occurs in the calculated values.

The adsorption studies show that CO_2 is stable on the bridge site of Ni(111); for all other sites, originally placed CO_2 moves to the neighboring bridge site though energy optimized CO_2 structures has significant differences compared to the bridge type adsorbed CO_2 (Table 4.1). The frequency analysis for 1/2 MLE on Ni(111) showed that stretching frequency of atop- CO_2 is the highest (2131.9 cm^{-1}) and it decreases down to 1997.2 cm^{-1} for the bridge type adsorption. Further decrease is observed when the adsorption type is changed to fcc and hcp, which have stretching frequencies of 1975.9 cm^{-1} and 1936.6 cm^{-1}, respectively. The decrease in surface concentration to 1/4 MLE led to a slight decrease in C-O frequency for atop, bridge and fcc type adsorption, whereas there is an increase in stretching frequency of CO_2 for hcp type adsorption.

Atop type CH_4 adsorption yields 1690.6 cm^{-1}C-H stretching frequency for 1/2 MLE surface concentration and it drastically increases to 2628.1 cm^{-1} with the decrease in surface concentration to 1/4 MLE. Similar increase is observed for bridge type adsorption, from 3035 cm^{-1} to 4260 cm^{-1}. On the other hand, the stretching frequency increases with an increase in CH_4 surface concentration, from 2415.1 cm^{-1} to 3687.1 cm^{-1}, for hcp type adsorption indicating strong effect of surface concentration change on the internal energy of the molecule. For fcc type adsorption, the stretching frequency is calculated as 3687.5 cm^{-1}, very close to that of hcp, for 1/2 MLE surface concentration. The lower surface concentration, 1/4 MLE, leads to a significant change in the methane structure, the C-H stretching frequency could not be calculated.

CH_3 adsorbed atop and bridge sites yields stretching frequencies in 3435-3500 cm^{-1} band for 1/2 MLE surface concentration. Though hcp-type adsorbed CH_3 has a closer stretching frequency, (3492 cm^{-1}), fcc type adsorbed CH_3 has drastically different stretching frequency as 3048.2 cm^{-1}. Except for the atop adsorption case, dilution of CH_3 on the surface leads to a decrease in stretching frequency values; this decrease is limited for fcc case, ie. from 3048.2 cm^{-1} to 3019.8 cm^{-1}, but it is very drastic for hcp case, from 3491.7 cm^{-1} to 3040.3 cm^{-1}. On the other hand, surface concentration decrease leads to a limited increase in C-H stretching frequency for atop bound CH_3, from 3491.4 cm^{-1} to 3508.8 cm^{-1}.

Atop bound CH_2 on Ni(111) for 1/2 MLE concentration has stretching frequency of 3243.4 cm^{-1}. The bridge and multifold-bound CH_2 on Ni(111) has significantly lower stretching frequency, in ca. 2855 cm^{-1} to 2920 cm^{-1} band. With the decrease in surface concentration to 1/4 MLE, stretching frequency of CH_2 for all types of adsorption decreases down to 2690 – 2740 cm^{-1} range.

CH adsorption on Ni(111), on the other hand, yields C-H stretching frequencies very close to each other, in the 2965 – 2980 cm^{-1} range, for all types of adsorption at 1/2 MLE. Decrease in surface concentration leads to a decrease by ca. 100 cm^{-1} for all adsorption types.

Table 4.5. Frequency of CO, CO_2, CH_4, CH_3, CH_2 and CH at all possible adsorption sites of Ni(111) surface, 2x2 supercell. Tabulated adsorption sites are the original sites before geometry optimization.

Molecule	**Adsorption Site**	**Frequency (cm^{-1}) for 1/2 MLE**	**Frequency (cm^{-1}) for 1/4 MLE**
CO	Atop	2099.0	2124.9
CO	Bridge	1971.0	2025.4
CO	Fcc	1975.2	1975.2
CO	Hcp	1987.2	1987.2
CO_2	Atop	2131.9	2126.6

Table 4.5. Frequency of CO, CO_2, CH_4, CH_3, CH_2 and CH at all possible adsorption sites of Ni(111) surface, 2x2 supercell. Tabulated adsorption sites are the original sites before geometry optimization (cont.).

Molecule	**Adsorption Site**	**Frequency (cm^{-1}) for 1/2 MLE**	**Frequency (cm^{-1}) for 1/4 MLE**
CO_2	Bridge	1997.2	1963.5
CO_2	Fcc	1975.9	1960.9
CO_2	Hcp	1936.6	1961.4
CH_4	Atop	1690.6	2628.1
CH_4	Bridge	3035.0	4260.0
CH_4	Fcc	3687.5	-
CH_4	Hcp	3687.7	2415.7
CH_3	Atop	3497.4	3508.8
CH_3	Bridge	3436.3	3312.1
CH_3	Fcc	3048.2	3019.8
CH_3	Hcp	3491.7	3040.3
CH_2	Atop	3243.4	2740.6
CH_2	Bridge	2861.4	2734.6
CH_2	Fcc	2858.8	2718.7
CH_2	Hcp	2917.3	2690.1
CH	Atop	2978.2	2870.2
CH	Bridge	2968.0	2858.4
CH	Fcc	2977.8	2874.8
CH	Hcp	2968.6	2863.7

The stretching frequencies calculated for CH_x molecules on possible adsorption sites of PtNi(111) surface alloy indicate the effect of Pt presence (Table 4.6). In general, adsorbed CH_4 molecules have far different stretching frequencies when they are placed on sites directly involving Pt, like atop Pt or a bridge site for which one leg of the adsorbate is on Pt atom. Adsorbed CH_4 molecule on the T4 site, which is atop Pt, has C-H stretching

frequency of 3684 cm^{-1} whereas CH_4 placed at T1, T1 and T3, which are all Ni-atop sites, has stretching frequency within the range 2530-2600 cm^{-1}. For the bridge type CH_4 adsorption, Pt is directly involved in B1 and B2 sites at which CH_4 stretching frequencies are calculated as 2186.1 cm^{-1} and 1980.2 cm^{-1}, respectively. On the other hand, there is an increase in C-H stretching frequency to 2708.1 cm^{-1} for CH_4 at bridge site B3, which has both legs at Ni but one of the Ni is directly coordinated with Pt. As it comes to CH_4 placed at B4, the stretching frequency assumes for greater values, 3686 cm^{-1}, as both Ni atoms at the site do not have any coordination with Pt. The only multifold adsorption site that does not directly have Pt is HCP1. As expected, the stretching frequency of CH_4 at HCP1, which is calculated as 3684.7 cm^{-1}, is far different from the values obtained from CH_4 at sites FCC1 and HCP2, which are 2786.8 cm^{-1} and 2572.7 cm^{-1}, respectively. Though there is a Pt at site FCC2, CH_4 at FCC2 yields a stretching frequency of 3685.4 cm^{-1}, which is very close to 3684.7 cm^{-1} calculated for site HCP1, indicating there may be a diffusion of CH_4 between the adsorption sites HCP1 and FCC2.

The calculated stretching frequency results indicate that CH_3 on all possible atop sites yields stretching frequencies in the 3475-3485 cm^{-1} range. For the bridge type adsorption of CH_3, direct Pt involvement at the site B1 and B2 leads to higher C-H stretching frequencies, 3481.5 cm^{-1} and 3501.9 cm^{-1}, respectively, compared to those at the B3 and B4 sites, yielding stretching frequencies of 3137.3 cm^{-1} and 3015.4 cm^{-1}, respectively, due to lack of direct Pt presence. CH_3 at multifold adsorption sites yield stretching frequencies in the range 3050 – 3140 cm^{-1} except the one at HCP2 site that has a stretching frequency of 3483.1 cm^{-1}.

Atop CH_2 adsorption yields stretching frequency is 2608.2 cm^{-1} for site T2, stretching frequencies are in the range of 2700 - 2750 cm^{-1} for sites T1 and T4, and 3037.8 cm^{-1} for site T3. Adsorption of CH_2 at the bridge sites yields C-H stretching frequencies as ca. 2800 cm^{-1} for B1, B2 and B3, whereas for adsorption at B4 the calculated frequency value decreases down to 2682.5 cm^{-1}. Similarly, adsorption on HCP2 type site yields slightly lower stretching frequency, 2674.6 cm^{-1}, while for the rest of the multifold adsorption sites, C-H stretching frequency is in 2800 - 2820 cm^{-1} range.

CH adsorption at atop sites shows that adsorption atop Pt and atop Ni leads similar C-H stretching frequency values; atop adsorption on Ni, the sites T1 and T2, and on Pt, site T4 yield stretching frequencies in 2900-2940 cm^{-1} range. The only atop site for which the C-H stretching frequency is lower is T3 with the value of 2726.6 cm^{-1}. CH adsorption on possible bridge and multifold type adsorption sites of PtNi(111) surface alloy yield C-H stretching frequencies ca. 2900 cm^{-1}.

In the FTIR-DRIFT analysis, CO can be used both as the probe molecule for detailed surface characterization of active metal sites, like the ones on PtNi, and as the molecule that enables understanding the surface mechanism of CO_2 dissociation to CO and O. Table 4.7 summarizes the result of the C-O stretching frequency analysis for adsorbed CO_2 and CO on possible sites of PtNi surface alloy. The sites for which the C-O stretching frequency values of the adsorbate are not given indicate that CO molecule on the site undergoes a significant geometry change, like the elongation of C-O bond.

CO molecule adsorbed atop on Ni and Pt has C-O stretching frequency in 2120 - 2140 cm^{-1} range except for the Ni-atop site T3 for which C-O stretching frequency is calculated as 2035.6 cm^{-1}.

No convergence for the CO adsorbed at the bridge sites B2 and B3 indicates C-O bond elongation that may lead disruption. The C-O stretching frequency calculated for CO adsorbed on bridge site B1, having one Pt and one Ni at its legs, is 2122.9 cm^{-1}.

Among the CO molecules placed on multifold adsorption sites, the ones at FCC1 and FCC2, both having one Pt and two Ni legs and symmetrical with respect to Pt, yield exactly the same C-O stretching frequency, 2122.5 cm^{-1}. CO at HCP2, which again has one Pt and two Ni legs, has a lower CO stretching frequency as 1970.9 cm^{-1}. CO adsorbed on the only multifold adsorption site which does not have any Pt leg, yields the stretching frequency of 2007.9 cm^{-1}.

Table 4.6. Frequency of CH_4, CH_3, CH_2 and CH at all possible adsorption sites of PtNi(111) surface alloy, 2x3 supercell. Tabulated adsorption sites are the original sites before geometry optimization.

Molecule	**Adsorption Site**	**Frequency (cm^{-1}) for 1/6 MLE**	**Molecule**	**Adsorption Site**	**Frequency (cm^{-1}) for 1/6 MLE**
CH_4	T1	2561.5	CH_2	T1	2747.3
CH_4	T2	2537.8	CH_2	T2	2608.2
CH_4	T3	2596.3	CH_2	T3	3037.8
CH_4	T4	3684.2	CH_2	T4	2709.1
CH_4	B1	2186.1	CH_2	B1	2800.5
CH_4	B2	1980.2	CH_2	B2	2800.7
CH_4	B3	2708.1	CH_2	B3	2797.4
CH_4	B4	3686.2	CH_2	B4	2682.5
CH_4	FCC1	2726.8	CH_2	FCC1	2802.7
CH_4	FCC2	3685.4	CH_2	FCC2	2820.6
CH_4	HCP1	3684.7	CH_2	HCP1	2803.1
CH_4	HCP2	2572.7	CH_2	HCP2	2674.6
CH_3	T1	3485.5	CH	T1	2941.3
CH_3	T2	3486.9	CH	T2	2916.8
CH_3	T3	3476.8	CH	T3	2726.6
CH_3	T4	3485.4	CH	T4	2901.5
CH_3	B1	3481.5	CH	B1	2900.8
CH_3	B2	3501.9	CH	B2	2901.3
CH_3	B3	3137.3	CH	B3	2901.3
CH_3	B4	3015.4	CH	B4	2902.7
CH_3	FCC1	3134.1	CH	FCC1	2901.7
CH_3	FCC2	3054.4	CH	FCC2	2917.0
CH_3	HCP1	3128.1	CH	HCP1	2900.7
CH_3	HCP2	3483.1	CH	HCP2	2905.3

According to the result of the CO_2 adsorption studies on PtNi(111) surface alloy sites, CO_2 originally placed on atop T1, T2, T3 and T4 sites are all diffused to the neighboring bridge sites. Similarly, CO_2 placed originally at multifold adsorption sites are diffused to the neighboring bridge sites. Among them, CO_2 originally placed on FCC1, FCC2 and HCP2 diffuse to the closest bridge sites, having one Ni and one Pt on their legs, whereas CO_2 originally placed on HCP1 diffuses to a bridge site B3 which has both Ni legs. It should be also noted based on the results of the adsorption studies that one C-O bonds of CO_2 originally placed at B1 elongates and oxygen moves away from the surface, and CO_2 does not interact with the surface when it is originally placed at B3. In accordance with the findings of the adsorption study, C-O stretching frequency of CO_2 at B1 does not converge as one of its C-O bonds is elongated. The stretching obtained for site B3, 1966.9 cm^{-1}, can be considered as the frequency when CO_2-surface interaction is insignificant. CO_2 placed at the adsorption sites B2 and B4, for which CO_2 adsorption is found stable, yield stretching frequency as 2191.1 and 2282.5 cm^{-1}, respectively. CO_2 placed on T3 and T4 has C-O stretching frequency of ca. 2191.5 cm^{-1}, almost equal to that of CO_2 placed at B2, verifying CO_2 diffusion from atop to bridge sites. CO_2 adsorbed at T1, on the other hand, yields stretching frequency of 2306.5 cm^{-1}, which is close to that of CO_2 at B4, which is 2282.5 cm^{-1}.

Among the CO_2 adsorbed on possible multifold adsorption sites, CO_2 on HCP1 yields C-O stretching frequency of 1972.8 cm^{-1} which is very close to that obtained from CO_2 on B3. It should be noted that CO_2 originally placed at HCP1 diffuses to B3 which then, according to the adsorption studies, leaves the surface. CO_2 at FCC1 yields C-O frequency of 1959 cm^{-1}, which, according to the adsorption studies, diffuses and is stabilized at B1, leading one oxygen leaves the surface. CO_2 at HCP2 has a C-O stretching frequency of 2120.3 cm^{-1}, which is very close to that obtained from adsorption on B2.

Table 4.7. Frequency of CO and CO_2 at all possible adsorption sites of PtNi(111) surface alloy, 2x3 supercell. Tabulated adsorption sites are the original sites before geometry optimization.

Molecule	**Adsorption Site**	**Frequency (cm^{-1}) for 1/6 MLE**	**Molecule**	**Adsorption Site**	**Frequency (cm^{-1}) for 1/6 MLE**
CO	T1	2120.7	CO_2	T1	2306.5
CO	T2	2123.1	CO_2	T2	-
CO	T3	2035.6	CO_2	T3	2191.5
CO	T4	2140.0	CO_2	T4	2190.0
CO	B1	2122.9	CO_2	B1	-
CO	B2	-	CO_2	B2	2191.1
CO	B3	-	CO_2	B3	1966.9
CO	B4	2017.4	CO_2	B4	2282.5
CO	FCC1	2122.5	CO_2	FCC1	1959.2
CO	FCC2	2122.5	CO2	FCC2	2037.4
CO	HCP1	2007.9	CO2	HCP1	1972.8
CO	HCP2	1970.9	CO2	HCP2	2120.3

5. CONCLUSIONS AND RECOMMENDATIONS

5.1. Conclusions

The results of the current study reveal that;

Although, CO_2 adsorption energies have positive values, there is an electronic interaction between the adsorbate and the surface for adsorption on Ni(111) sites.

CO_2 adsorption on Ni(111) surface is stable only on the bridge site; CO_2 placed on the other sites diffuse to the bridge site upon energy optimization.

CO_2 adsorption is unstable on the atop and multifold sites of PtNi(111) surface alloy; CO_2 molecule originally placed on those sites diffuse to the neighboring bridge sites.

CO_2 adsorbed on the bridge sites of PtNi(111) has an ability to produce surface oxygen, as calculations indicated for the adsorption on B1 site of PtNi surface alloy, which has one Pt and one Ni legs.

CO adsorption is stable on all sites of Ni(111), whereas oxygen adsorption is only stable on the multifold sites.

The results of the frequency analysis confirm the findings of the adsorption studies.

Frequency analysis results clearly show the pronounced effect of Pt presence on the adsorption properties of the PtNi surface alloy and the internal energy of the adsorbate molecules.

5.2. Recommendations

Further studies should be focused on detailed investigation of properties of PtNi surface alloy. In this context, a detailed adsorption/coadsorption study having Pt concentration of PtNi surface alloy and surface coverage of the adsorbates as the parameters should be conducted. Upon the determination of the most favorable adsorption sites, the changes in surface mechanism in response to Pt defect concentration and adsorbate surface concentration should be investigated, and links should be established between the theoretical and experimental mechanistic studies.

REFERENCES

Alonso, D. S.J., J. J. Juan. M. J. I. Gomez. M. C. R. Martinez, 2009, "Ni, Co and Bimetallic Ni–Co Catalysts for the Dry Reforming of Methane", *Applied Catalysis A: General*, Vol. 371, pp. 54-59.

Akpan, E., Y. Sun, P. Kumar, H. Ibrahim, A. Aboudheir and R. Idem, 2007, "Kinetics, Experimental and Reactor Modeling Studies of The Carbon Dioxide Reforming of Methane (CDRM) Over a New Ni/CeO_2–ZrO_2 Catalyst in a Packed Bed Tubular Reactor" *Chemical Engineering Science*, Vol. 62, pp. 4012 – 4024.

Aydinoglu. S., E. Ozensoy. A. E. Aksoylu, 2009, "The Effect of Impregnation Strategy on Methane Dry Reforming Activity of Ce Promoted Pt/ZrO_2", *International Journal of Hydrogen Energy,* Vol. 34, pp. 9711 – 9722.

Aydinoglu. S., and A. E. Aksoylu, 2011, "CO_2 Reforming of Methane Over Pt-Ni/Al_2O_3 Catalysts: Effects of Catalyst Composition and Water and Oxygen Addition To The Feed", *International Journal of Hydrogen Energy*, Vol. 36, pp. 2950-2959.

Cheng, J., W. Huang, 2010, "Surface Modification of Ni Catalysts with Trace Pt for Oxidative Steam Reforming of Methane", *Journal of Catalysis*, Vol. 245, pp. 144–155.

Choe, S. J., H. J. Kang, D. H. Park, D. S. Huh, J. Park, 2001, "Adsorption and Dissociation Reaction of Carbon Dioxide on Ni(111) Surface: Molecular Study", *Applied Surface Science,* Vol. 181, pp. 265-276

Cook, D.B., 2005, *Handbook of Computational Quantum Chemistry*, Dover Publications Inc., NewYork.

Das, N.K. and T. Shoji, 2011, "A Density Functional Study of Atomic Oxygen and Water Molecule Adsorption on Ni(111) and Chromium-Substituted Ni(111) surfaces", *Applied Surface Science*, Vol. 258, pp. 442– 447.

Delly, B., 1990, "An All-electron Numerical Method for Solving the Local Density Functional for Polyatomic Molecules", *Journal of Chemical Physics,* Vol. 92, pp. 508.

Delly, B., 2000, "From Molecules to Solids with the DMol3 Approach", *Journal of Chemical Physics*, Vol. 113, pp. 7756.

Diéguez, M. G., E. Finocchio, M. Á. Larrubia, L. J. Alemany and G. Busca, 2010, "Characterization of Alumina-Supported Pt, Ni and PtNi Alloy Catalysts for the Dry Reforming of Methane", *Journal of Catalysis*, Vol. 274, pp. 11–20.

Diéguez, M. G.,, I.S. Pieta, M.C. Herrera, M.A. Larrubia and L.J. Alemany, 2010, "Improved Pt-Ni Nanocatalysts for Dry Reforming of Methane", *Applied Catalysis A: General*, Vol. 377, pp. 191–199.

Fidalgo, B., L. Zubizarreta, J.M. Bermúdez, A. Arenillas and J.A. Menéndez, 2010, "Synthesis of Carbon-Supported Nickel Catalysts for The Dry Reforming of CH_4", *Fuel Processing Technology,* Vol. 91, pp. 765–769.

Formoso, V., A. Marino, G. Chiarello, R.G. Agostino, T. Caruso, E. Colavita, 2006, "CO Adsorption on Ni(1 0 0): Evidences for a Weakly Bound Phase by HREELS Measurements", Surface Science, Vol.600, pp.1456-1461.

Gamba, O., S. Moreno and R. Molina, 2011, "Catalytic Performance of Ni-Pr Supported on Delaminated Clay in the Dry Reforming of Methane", *International Journal of Hydrogen Energy*, Vol. 36, pp. 1540-1550.

Gautam, S., K. Dharamvir, N. Goel, 2013, "CO_2 Adsorption and Activation Over Medium Sized Cu_n (n = 7, 13 and 19) Clusters: A Density Functional Study", *Computational and Theoretical Chemistry*, Vol. 1009, pp. 8–16.

Gosson, M., 2001, *The Principles of Newtonian and Quantum Mechanics*, Imperial College Press., London.

Ito, M., T. Tagawa, S. Goto, 1999, "Suppression of Carbonaceous Depositions on Nickel Catalyst for the Carbon Dioxide Reforming of Methane", *Applied Catalysis A: General*, Vol. 177, pp. 15-23.

Kang, K. M., H. W. Kim, I. W. Shim and H. Y. Kwak, 2011, "Catalytic Test of Supported Ni Catalysts with Core/Shell Structure for Dry Reforming of Methane", *Fuel Processing Technology*, Vol. 92, pp. 1236–1243.

Luna, A. E. C., M. E. Iriarte, 2008, "Carbon Dioxide Reforming of Methane Over a Metal Modified Ni-Al_2O_3 Catalyst", *Applied Catalysis A: General*, Vol. 343, pp. 10–15.

Nikolla, E., J. Schwank and S. Linic, 2009, "Comparative Study of The Kinetics of Methane Steam Reforming on Supported Ni and Sn/Ni Alloy Catalysts: The Impact of the Formation of Ni Alloy on Chemistry", *Journal of Catalysi,* Vol. 263, pp. 220–227.

Materials Studio Release Notes, Reprinted with permission from Accelrys Software Inc., San Diego, 2008, http://list.cineca.it/, accessed at December 2012.

Material Studio Software, 2011, Accelrys Software Inc.. San Diego.

Materials Studio Overview, 2011, Reprinted with permission from Accelrys Software Inc., Accelrys Software Inc.. San Diego, http://accelrys.com/products/datasheets/materials-studio-overview.pdf, accessed at December 2012.

Michaelides, A. and P. Hu, 1999, "Methyl Adsorption on Ni(111) and C-H-M Multicentre Bonding: A Density Functional Theory Study", *Surface Science*, Vol. 437, pp. 362–376.

Michaelides, A. and P. Hu, 2000, "A Density Functional Theory Study of CH_2 and H Adsorption on Ni(111)", *Journal of Chemical Physics*, Vol. 112, pp.13.

Michaelides, A. and P. Hu, 2000, "A First Principles Study of CH_3 Dehydrogenation on Ni (1 1 1)", *Journal of Chemical Physics*, Vol. 112, pp.18.

Padama, A. A., H. Kasai and H. Kawai, 2012, "The Mechanism of H_2 Dissociation and Adsorption on Mn-Modified Ni(111) Surface: A Density Functional Theory-Based Investigation", *Surface Science*, Vol. 606, pp. 62–68.

Parvary, M., S.H. Jazayeri, A. Taeb, C. Petit, A. Kiennemann, 2001, "Promotion of Active Catalysts in Methane Dry Reforming Reaction by Aluminum Addition", *Catalysis Communication*, Vol.2, pp. 357-362.

Pawelec, B., S. Damyanova, K. Arishtirova, J.L.G. Fierro and L. Petrov, 2007, "Structural and Surface Features of PtNi Catalysts for Reforming of Methane with CO_2", *Applied Catalysis A: General*, Vol. 323, pp. 188–201.

Pedersen, F. A., O. Lytken, J. Engbæk, G. Nielsen, I. Chorkendorff and J. K. Nørskov, 2005, "Methane Activation on Ni(111): Effects of Poisons and Step Defects", *Surface Science,* Vol. 590, pp. 127–137.

Pick, S., 2007, "Density-Functional Study of The Co Adsorption on Ferromagnetic Co(0001) and Co(111) Surfaces", *Surface Science*, Vol. 601, pp. 5571–5575.

Pietraszek. A., B. Koubaissy, A. C. Roger and A. Kiennemann, 2011, "The Influence of the Support Modification Over Ni-Based Catalysts for Dry Reforming of Methane Reaction", *Catalysis Today*, Vol. 176, pp. 267– 271.

Pistonesi, C., A. Juan, B. Irigoyen and N. Amadeo, 2007, "Theoretical and Experimental Study of Methane Steam Reforming Reactions Over Nickel Catalyst Ni(1 1 1)", *Applied Surface Science,* Vol. 253, pp. 4427–4437.

Quiroga, M. M., A. E. Castro-Luna, 2010, "Catalytic Activity and Effect of Modifiers on Ni-Based Catalysts for the Dry Reforming of Methane", *International journal of Hydrogen Energy*, Vol. 35, pp. 6052 – 6056.

Seminario, J.M., 1996, *Recent Developments and Applications of Modern Density Functional Theory*, Elsevier. New York.

Schilbe, P., S. Siebentritt, K.-H. Rieder, 1995, "Adsorption of CO on Ni (311). Investigations with HREELS", Chemical Physics Letters, Vol.233, pp.569-574.

Sholl, D. S., J. A. Steckel, 2009, *Density Fucntional Theory*, Wiley, New Jersey.

Wang, S., D. Cao, Y. W. Li, J. Wang and H. Jiao, 2006, "CH_4 Dissociation on Ni Surfaces: Density Functional Theory Study Ni(111), Ni (100), Ni(110)", *Surface Science*, Vol. 600, pp. 3226–3234.

Wang, S., X. Yuan, J. Hu, D. B. Cao, Y. W. Li, J. Wang and Haijun Jiao, 2007, "Kinetic Aspect of CO_2 Reforming of CH_4 on Ni(111): A Density Functional Theory Calculation", *Surface Science,* Vol. 601, pp. 1271–1284.

Wang, X. , N. Wang, J. Zhao and L. Wang, 2010, "Thermodynamic Analysis of Propane Dry and Steam Reforming for Synthesis Gas or Hydrogen Production", *International Journal of Hydrogen Energy*, Vol. 35, pp. 12800-12807.

Watwe, R. M. , H. S. Bengaard, J. R. Rostrup-Nielsen, J. A. Dumesic, and J. K. Nørskov, 2000, "Theoretical Studies of Stability and Reactivity of CHx Species on Ni(111)", *Journal of Catalysis*, Vol. 189, pp. 16–30.

Vannice, M.A, 1982, "Catalytic Activation of Carbon Monoxide on Metal Surfaces", *Catalysis-Science and Technology*, Vol. 3, pp. 139-198.

Yang, H., Whitten J.L., 1996, "Adsorption of CNH_2 and HCNH on the Ni(111) Surface", *Chemical Physics Letters*, Vol.251, pp.20-25.

Yates, J. T. and J. K. Joh,nson, 2007, *Molecular Physical Chemistry for Engineers*, University Science Books, Sausalito, California.

Yoshinobu and Kawai, 1996, "Site Occupation of Adsorbed CO on Ni(100)", *Springer Series in Solid-State Sciences*, Vol.121, pp.78-85.

Zhu, Y. A., X. G. Zhou, D. Chen and W. K. Yuan, 2007, "First-Principles Study of C Adsorption and Diffusion on the Surfaces and in the Subsurfaces of Nonreconstructed and Reconstructed Ni(100)", *J. Phys. Chem.,* Vol. 111, pp. 3447-3453.

Zhu, Y.A., D. Chen, X. G. Zhou and W. K. Yuan, 2009, "DFT Studies of Dry Reforming of Methane on Ni Catalyst Ni(1 1 1)", *Catalysis Today*, Vol. 148, pp. 260–267.

Zuo, Z., W. Huang, P. Han and Z. Li, 2010, "A Density Functional Theory Study of CH_4 Dehydrogenation on Co(1 1 1)", Applied Surface Science, Vol. 256, pp. 5929–5934.